Iwate University
Doctoral dissertation

Localization of Human Bodies Using Array-Based Bio-Radar with Imperfect RF Devices

Graduate School of Science and Engineering
ABUDUSAIMI ABUDUAINI
March, 2024

Contents

Chapter 1

Introduction

1.1 Social background
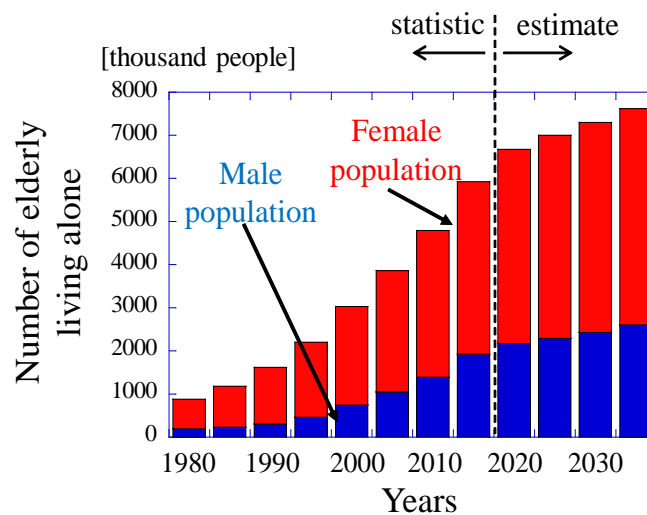
Figure 1.1: Trends of the elderly population living alone

Recently, the COVID-19 pandemic has had a widespread impact, highlighting the issue of staying indoors demand. Furthermore, with the advent of an aging society, the number of elderly people living alone is increasing in Japan. Fig.1.1 shows the trends of elderly people living alone, and it can be seen that this increasing phenomenon will remain for decades. There has been a corresponding rise in the incidence of accidental falls in elderly households, and the concerning problem of isolated deaths among the need for direct contact with the human body handicaps the latter global scale. As a result, there is a growing need for systems that can efficiently monitor the safety of the elderly.

1.2 Conventional safety monitoring system for the elderly

There are a variety of monitoring systems available with many features for the care of the elderly [1]∼[5]. For example, internet-enabled security cameras have made it possible to see our elder parents from any part of the world on our smartphones or computers [6]. Gadgets with GPS and motion sensor-enabled devices are available in a smartwatch or a bracelet to detect the location of a patient or to detect if the patient had any fall, in case of an emergency they have a panic button.[7]. Although these systems are easy to deploy, however, the former has problems with privacy violations in private places like bathrooms and toilets, moreover, They tend to have blind areas behind a large object. The latter one is directly attached to the human body, where it will cause contact restrictions, discomfort, and increased mental burden due to restraint. Moreover, there are also health problems caused by long-term use. Furthermore, it is inconvenient for elderly people because of the charging problem. By considering these reasons, a safety monitoring system that can monitor the health status and location of the elderly without these issues is required.

1.3 Biological position estimation technology using microwave

In Chapter 1.2, we have discussed the existing issues of conventional safety monitoring systems for the elderly. In addressing this demand, the use of wireless biomedical sensors for safety monitoring has garnered significant attention [43]∼[46]. Unlike traditional safety monitoring systems, this approach does not violate privacy, and body contact is unnecessary. Furthermore, these studies investigated the possibility of detecting physiological parameters without any contact and achieved the monitoring of vital signs. Breathing and heart rates are two of the most studied physiological parameters for creating contactless sensors [47]∼[50]. Fluctuations in the superficial arteries are linked to heart activity, whereas the principal function of the respiratory system is to exchange gases from the inside to the outside of the body. In this context, the use of radar sensors for noncontact detection of the Doppler effect caused by human-body motion (e.g., respiration) has emerged as an interesting research topic fueled by tremendous technological advancements [51]∼[55]. In this field, a vital sign observation method using multiple-input multiple-output (MIMO) and single-input multiple-output (SIMO) radar technology has been proposed [56]∼[62].

MIMO radars are classified into two types based on the configuration of their transmitting and receiving antennas: monostatic and bistatic. Monostatic MIMO radars typically require a relatively large bandwidth. By contrast, bistatic MIMO radars require only a narrowband continuous-wave (CW)

signal. Moreover, they have been widely studied because of their known capabilities in (i) improving the precision and dependability of vital sign detection [63], [64] and (ii) providing good positioning accuracy of human-body locations. Bistatic MIMO radar localization [65]~[67] is also an essential topic in safety monitoring applications. These MIMO radars observe the signals Doppler-shifted by human activity and estimate both the directions of departure (DoD) and direction of arrival (DoA). Human-body locations can be estimated by determining the intersection points in these two directions. Related works have presented an improved DOA/DOD estimation method suitable for human body localization that uses bistatic MIMO radar [15]-[18]. Chen et al. [15] adjusted the DOA/DOD estimation model by solving the unknown mutual coupling effect between antennas. Wen et al. [16] compared different estimation algorithms and proposed a covariance-based trilinear decomposition estimator. Tang et al. [17] proposed another novel grid-free DOD and DOA estimation algorithm. Gong et al. [18] utilizes an improved U-ESPRIT algorithm to estimate DOD and DOA jointly. These works only focused on the direction-finding problem and estimation algorithms. Unfortunately, the existing version of these methods assumes the ideal situation, e.g., transmitter and receiver are fully synchronized [19]. E. Cardillo and A. Caddemi [20] reviewed and discussed the existing MIMO technologies and their application to vital sign detection and human localization.

Among the state-of-the-art publications listed, most of the reported biomedical MIMO radars are monostatic, very few publications describe bistatic variants, and with regard to the bistatic MIMO radars mentioned, none of the listed papers addressed the frequency difference between the transmitter and receiver. They assumed no frequency differences between the transmitter and receiver. But in actual use, to reduce the cost of the radar system and suit the bistatic MIMO radar, it is desirable to use commercially available devices. For example, utilizing cheap Wi-Fi chips at the transmitter and receiver sides significantly reduces the cost of the radar system. With the spread of Wi-Fi-equipped with multiple antennas to support bistatic MIMO systems, using antenna array-based technology for indoor localizing is attracting attention. Sasakawa *et al.*. [21] proposed a method that can localize the targets ' (up to three) positions within a few seconds. This method uses the time-differential MIMO channel, created by cyclic human activities such as respiration and heartbeat. This MIMO radar can estimate target position faster and accurately. However, this method requires the antennas to be calibrated due to the phase error caused by the radio frequency (RF) front end. Sasakawa *et al.*. [22] have also proposed an antenna array calibration method. This method uses the SIMO channel, and living body direction can be estimated by aDOAdetermination method. The proposed method does not require any hardware for calibration, and the phase error due to the RF front end is estimated and fixed

from known subject direction information gathered in a calibration step. Though this calibrated array antenna can estimate living-body direction within an acceptable range of error, the resulting radar system is unable to localize living bodies. Moreover, this calibration method can only offset the phase error caused by RF front end, and fails to remove the time-varying phase errors that exist between the transmitters and receivers.

Frequency synchronization is always a big challenge for bistatic MIMO radar [23, 24] since the transmitter and receiver have their own oscillators with different clock frequencies due to the limited accuracy of commercial devices. The localization performance with separated radar units was discussed in [25]. Although the author of [25] proposed solutions to estimate and correct local oscillator drift and phase noise, wide bandwidth is needed to compensate for the frequency and phase drift and only FMCW radars are supported. D. Liang *et al.* [26, 27] proposed a synchronization phase-error estimation and compensation method suitable for bistatic synthetic aperture radar (BiSAR). However, the proposed scheme is for satellites, not for commercial off-the-shelf (COTS) based radar systems. These synchronization methods impose additional, expensive hardware requirements at the receiver. To achieve higher frequency accuracy and better localization performance from bistatic radars, some techniques that adopt stable and highly accurate references, such as the Global Positioning System (GPS) based clock synchronization system, have been studied [28, 29]. However, though GPS has high outdoor localization accuracy, it requires expensive hardware equipment on both sides and cannot be applied to indoor environments because the GPS signal is not available in most indoor environments. P. M. Marques *et al.* [30] proposed a low-cost passive bistatic radar, using commercial off-the-shelf (COTS) components. This study used two commercial devices with independent local oscillators. This system meets the low-cost requirement, and it can detect metallic objects with a range of up to 50 meters in an outdoor situation. However, indoor localization performance has not been tested. Moreover, their frequency accuracy is quite low due to the use of quartz crystal oscillators. Therefore, the frequency error between the transmitter and receiver remains a severe problem for low-cost bistatic MIMO radar. In particular, the frequency difference between transmitter and receiver severely degrades detection performance because the Doppler shift created by human body movement is extremely small and cannot be correctly detected. Therefore, a method that allows unsynchronized systems to estimate target locations in indoor environments accurately is needed.

As we discussed above, to achieve a low cost for a localization system, another option is to utilize the SIMO-based radar approach using COTS devices. It is often more budget-friendly compared to specialized MIMO hardware, which can significantly reduce the overall implementation cost. Moreover,

SIMO-based COTS devices are readily available and can be relatively easy to integrate into existing systems, especially since the devices do not have a full RF chain that is, only a single antenna can transmit the signal, simplifying the implementation process.

J. Xiong et al. [69] presented a CW-SIMO radar with a digital beamforming (DBF) technique for detecting multitarget vital signs. S. Shi et al. proposed a COTS-based system that can detect a person's respiration rate in dynamic ambient environments using a single transmitter (TX) and receiver (RX) pair of Wi-Fi stations [70]. Although these approaches can detect information on vital signs, their position estimation has not been thoroughly investigated. Significantly few studies on human-target localization using SIMO radar have been mentioned [71, 72] because SIMO radars only have the capability of DoA finding owing to the lack of channel information, and position detection is always a significant challenge. Ref. [71] proposed a single-frequency continuous-wave Doppler radar sensor implemented with a redundant SIMO architecture to precisely localize an indoor target. The described 2-D motion imaging algorithm was derived by computing the intersection points of three elliptical surfaces based on the spatial coordinates of the transmitting and receiving antennas with a specified imaging plane. However, this method is only effective when the target distance is comparable to the antenna aperture width. This implies that this method can only localize nearby targets. Ref.[72] proposed a telescopic structure-based SIMO ultra-wideband (UWB) radar with an improved method for detecting and locating multiple human targets under through-wall conditions. Although this approach includes only one transmitting antenna and three receiving antennas integrated with a telescopic structure for simplicity and portability, it requires a relatively large bandwidth. Moreover, the transmitter and receiver share the same oscillator. By contrast, in the COTS-based bistatic system, the transmitter and receiver are physically separated when utilizing two stations as transceivers because of the limitations of clock accuracy in their individual oscillators, where the frequencies of each station are inherently different. The phase error between the two stations strongly affects the localization accuracy; however, such a situation has not been considered.

1.4 Purpose of this study

As mentioned in the previous section, to reduce the cost of the radar system and suit the bistatic bio-radar, it is desirable to use commercially available imperfect RF devices. However, in such a COTS-based bistatic system, the transmitter and receiver are physically separated when utilizing two stations as transceivers because of the limitations of clock accuracy in their individual oscillators, where the frequencies of each station are inherently different. The phase error between the two stations strongly

affects the localization accuracy.

This study aims to propose and experimentally evaluate a frequency offset elimination technique suitable for MIMO and SIMO/MISO array-based bio-radar systems using imperfect RF devices, to achieve human-bodies localization in an indoor environment.

1.5 Structure of this thesis

Figure 1.2 shows the structure of this paper.

In chapter one, the technical background of modern detection systems is introduced, and the existing problems with these systems are discussed. Then the effectiveness of the bistatic MIMO radar in safety confirmation applications is mentioned. Also, the realization of localization using bistatic SIMO radar is discussed. To reduce the cost problems, the problems in bistatic MIMO and SIMO radar using imperfect RF devices for localization are listed. Among the raised problems, the target of this study was frequency offset elimination between the transmitter and receiver and target detection concerning the importance of realizing this system.

In chapter two, we present and experimentally evaluate a frequency error elimination technique suitable for unsynchronized bistatic MIMO radar for human-body detection.

In chapter three, we introduce an accurate human-body localization using a roundtrip SIMO channel and a frequency error elimination technique for the roundtrip channel between two stations is proposed.

In chapter four, a living-body positioning technique that integrates Time-of-flight (ToF) and Direction of Departure (DoD) utilizing real Wi-Fi stations is analyzed.
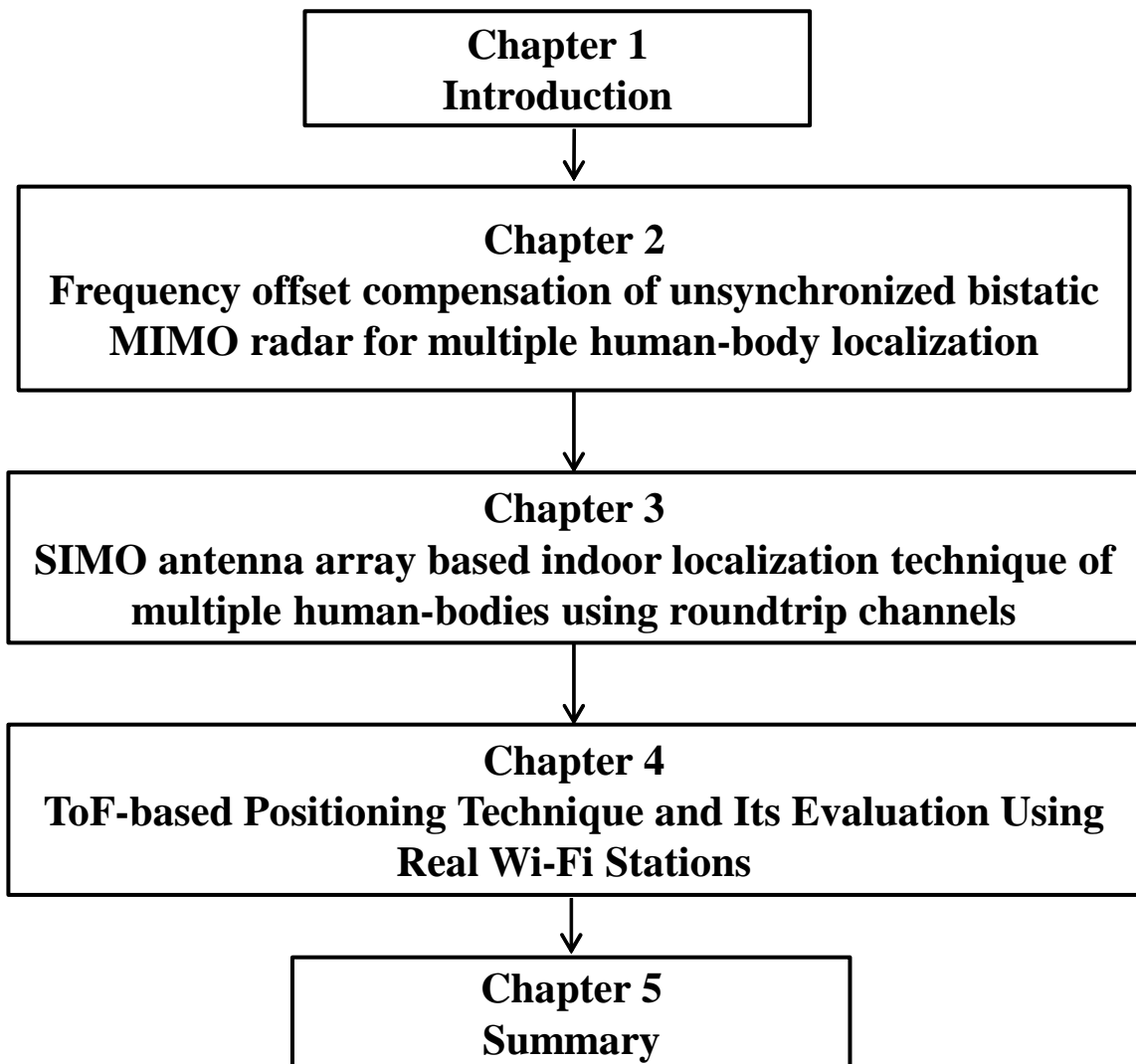
Chapter five is a summary.

```
┌─────────────────────────────────────────────┐
│                 Chapter 1                   │
│                Introduction                 │
└─────────────────────────────────────────────┘
                      │
                      ▼
┌─────────────────────────────────────────────────────────┐
│                       Chapter 2                         │
│  Frequency offset compensation of unsynchronized bistatic│
│        MIMO radar for multiple human-body localization  │
└─────────────────────────────────────────────────────────┘
                      │
                      ▼
┌─────────────────────────────────────────────────────────┐
│                       Chapter 3                         │
│ SIMO antenna array based indoor localization technique of│
│        multiple human-bodies using roundtrip channels   │
└─────────────────────────────────────────────────────────┘
                      │
                      ▼
┌─────────────────────────────────────────────────────────┐
│                       Chapter 4                         │
│  ToF-based Positioning Technique and Its Evaluation Using│
│                  Real Wi-Fi Stations                    │
└─────────────────────────────────────────────────────────┘
                      │
                      ▼
┌─────────────────────────────────────────────┐
│                 Chapter 5                   │
│                  Summary                    │
└─────────────────────────────────────────────┘
```

Figure 1.2: Structure of this study

Chapter 2

Frequency offset compensation of unsynchronized bistatic MIMO radar for multiple human-body localization

2.1 Frequency offset compensation of unsynchronized bistatic MIMO radar for multiple human-body localization

This section starts by reviewing human body localization based on bistatic CW-MIMO radar, then discusses some technical issues in COTS-based bistatic MIMO radar. Next the frequency error elimination technique based on target detection is discussed. Finally, simulation and experimental results are analyzed.

2.1.1 Review of human body localization using bistatic MIMO radar

The authors have investigated the performance of bistatic-CW MIMO radar for living-body localization in a multipath environment [55]. The target detection method is reviewed below.

Fig.2.1 shows the concept of human-body localization using bistatic MIMO radar. The proposed method uses M_R and M_T element antennas at the receiver and transmitter sides, respectively. The observed $M_R \times M_T$ time-variant MIMO channel is written as

$$\boldsymbol{H}(t) = \begin{pmatrix} h_{11}(t) & \dots & h_{1M_T}(t) \\ \vdots & \ddots & \vdots \\ h_{M_R 1}(t) & \dots & h_{M_R M_T}(t) \end{pmatrix}, \tag{2.1}$$

where, h_{ij} is the complex channel response from the j-th transmitter to the i-th receiver, and t represents the time of channel observation. This response is converted into a $M_R M_T \times 1$ virtual SIMO
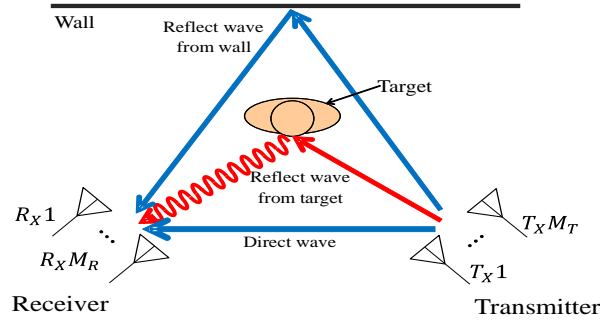
Figure 2.1: Concept of MIMO radar for human identification.

(Single-Input Multiple-Out) channel as follows

$$\boldsymbol{h_{11}}(t) = [h_{11}(t), \cdots, h_{M_R 1}(t), h_{21}(t), \cdots, h_{M_R M_T}(t)]^T. \tag{2.2}$$

Due to the multi-path environment, there are some unwanted paths that interfere with target localization. Therefore, to extract the frequency components corresponding to just the vital signs, the channel is Fourier-transformed to yield

$$\boldsymbol{F}(f) = [h_{11}(f), \cdots, h_{M_R 1}(f), h_{21}(f), \cdots, h_{M_R M_T}(f)]^T. \tag{2.3}$$

The correlation matrix using frequency response at the receiver side is expressed as,

$$\boldsymbol{R}_{FF} = \overline{\boldsymbol{F}(f)\boldsymbol{F}(f)^H}(f_1 < f < f_2), \tag{2.4}$$

where, f_1 and f_2 are the frequency range containing the influence of the vital signs; $\{\cdot\}^H$ represents the complex conjugate transposition. Eigenvalue decomposition yields both the eigenvector matrix and eigenvalue. Finally, using the steering vectors corresponding to DOD and DOA, we can find the peak values of the 2-dimensional MUSIC spectrum. Living-body locations can be estimated by finding the intersection points of these two directions [55]. The MUSIC method requires knowledge of the number of targets and we assume this information is known [42]. Theoretically, using the MUSIC algorithm to detect sources has an upper limit on the number of detected sources determined by the number of the receiving and transmitting antenna elements. In this case, the limit is $M_R \times M_T - 1$. If the number of antenna increases, more channel information becomes available, and more sources can be detected.

2.1.2 Technical issues in COTS-based bistatic MIMO radar

The preceding section mentioned the theoretical method for the human body localization using bistatic MIMO radar. However, in the actual performance, despite the aforementioned advantages, this radar

has also significant issues to be solved. The most important issue is the frequency synchronization between the transmitter and receiver because it causes the degradation of multiple target detection. The discussion of these problems is as follows.

Ensuring frequency synchronization is crucial for accurately detecting signals. Yet, in practical scenarios, commercially available devices are employed, leading to challenges. Specifically, the frequency variance between the transmitter and receiver significantly hampers signal detection by failing to accurately capture the Doppler shift caused by the human body. The separation of transmitters and receivers in bistatic systems results in individual oscillators with inherently different frequencies due to clock accuracy limitations. While signal processing effectively removes frequency offsets in communication systems, it inadvertently eliminates the intended Doppler shift caused by targets, thereby undermining target localization performance.

Detecting multiple targets presents distinct challenges compared to single target estimation. The complexities arise from uncertainties, leading to compromised localization performance caused by an unknown number of targets, limitations in antenna count resulting in missing targets, and increased disruption from the multipath channel. Consequently, the multitarget tracking problem remains a substantial challenge due to these intricate and varied factors.

2.2 Frequency offset elimination

Assuming the frequency of the transmitter platform is f_T, and the oscillator frequency of the receiver platform is f_R. Since the bistatic system's transmitter and receiver are separated, the transmitter and receiver have individual oscillators, and their frequencies are inherently different ($f_T \neq f_R$) due to clock accuracy limits. The frequency deviation between the two oscillators Δf is:

$$\Delta f(t) = f_T(t) - f_R(t). \tag{2.5}$$

The observed $M_R \times M_T$ time-variant MIMO channel with phase difference introduced by frequency deviation can be expressed as

$$\boldsymbol{H}(t) = \begin{pmatrix} h_{11}(t) & \cdots & h_{1M_T}(t) \\ \vdots & \ddots & \vdots \\ h_{M_R 1}(t) & \cdots & h_{M_R M_T}(t) \end{pmatrix} \exp(2\pi j \Delta f(t)). \tag{2.6}$$

The observed channel can be written as

$$\boldsymbol{H}(t) = \{\boldsymbol{H}_{\text{fix}} + \boldsymbol{H}_{\text{vital}}(t)\} \exp(2\pi j \Delta f(t)) + \boldsymbol{H}_{\text{noise}}(t), \tag{2.7}$$

11

where $\boldsymbol{H}_{\text{fix}}$ and $\boldsymbol{H}_{\text{vital}}(t)$ represent fixed channel and micro-Doppler channel due to human body's displacement, respectively. $\boldsymbol{H}_{\text{noise}}$ is the noise component due to the thermal noise. Note that $\boldsymbol{H}_{\text{vital}}(t)$ does not have a constant component, which is included in $\boldsymbol{H}_{\text{fix}}$, and we assume $E\left[\boldsymbol{H}_{\text{vital}}(t)\right] \simeq 0$. $\boldsymbol{H}_{\text{fix}}$ mainly consists of the direct path because we assume that the transmitter and the receiver are in a line-of-sight (LOS).

In this paper, the $\boldsymbol{H}_{\text{fix}}$ is used to eliminate the phase error in the channel because we can estimate phase rotation if $\boldsymbol{H}_{\text{fix}}$ is known. Even though the accurate information of $\boldsymbol{H}_{\text{fix}}$ is not available, we can approximately estimate the eigenpath of the $\boldsymbol{H}_{\text{fix}}$ by computing the correlation matrix instead of knowing $\boldsymbol{H}_{\text{fix}}$. The correlation matrix at the receiving side is described as

$$
\begin{aligned}
\boldsymbol{R}_{M_R} =& E\left[\boldsymbol{H}(t)\boldsymbol{H}(t)^H\right] \\
=& E\Bigg[\Big[\left\{\boldsymbol{H}_{\text{fix}} + \boldsymbol{H}_{\text{vital}}(t)\right\}\exp(2\pi j\Delta f(t)) + \boldsymbol{H}_{\text{noise}}(t)\Big] \\
&\quad \Big[\left\{\boldsymbol{H}_{\text{fix}}^H + \boldsymbol{H}_{\text{vital}}^H(t)\right\}\exp(-2\pi j\Delta f(t)) + \boldsymbol{H}_{\text{noise}}^H(t)\Big]\Bigg] \\
=& E\Big[\Big\{\boldsymbol{H}_{\text{fix}}\boldsymbol{H}_{\text{fix}}^H + \boldsymbol{H}_{\text{vital}}(t)\boldsymbol{H}_{\text{fix}}^H + \boldsymbol{H}_{\text{fix}}\boldsymbol{H}_{\text{vital}}^H(t) \\
&\quad + \boldsymbol{H}_{\text{vital}}(t)\boldsymbol{H}_{\text{vital}}^H(t)\Big\} \\
&\quad + \boldsymbol{H}_{\text{noise}}(t)\left\{\boldsymbol{H}_{\text{fix}}^H + \boldsymbol{H}_{\text{vital}}^H(t)\right\}\exp(-2\pi j\Delta f(t)) \\
&\quad + \left\{\boldsymbol{H}_{\text{fix}} + \boldsymbol{H}_{\text{vital}}(t)\right\}\exp(2\pi j\Delta f(t))\boldsymbol{H}_{\text{noise}}^H(t) \\
&\quad + \boldsymbol{H}_{\text{noise}}(t)\boldsymbol{H}_{\text{noise}}^H(t)\Big] \\
\simeq& E\left[\boldsymbol{H}_{\text{fix}}\boldsymbol{H}_{\text{fix}}^H\right] + E\left[\boldsymbol{H}_{\text{vital}}(t)\boldsymbol{H}_{\text{vital}}^H(t)\right] \\
&\quad + E\left[\boldsymbol{H}_{\text{noise}}(t)\boldsymbol{H}_{\text{noise}}^H(t),\right]
\end{aligned}
\tag{2.8}
$$

where the phase rotation is ideally eliminated in the correlation matrix. Also $E\left[\boldsymbol{H}_{\text{noise}}(t)\boldsymbol{H}_{\text{noise}}^H(t)\right] = \sigma_n^2\boldsymbol{I}$ because the noise component is assumed to be identically distributed and zero-mean Gaussian white. $[\boldsymbol{H}_{\text{noise}}(t)\left\{\boldsymbol{H}_{\text{fix}}^H + \boldsymbol{H}_{\text{vital}}^H(t)\right\}\exp(-2\pi j\Delta f(t))] = E[\left\{\boldsymbol{H}_{\text{fix}} + \boldsymbol{H}_{\text{vital}}(t)\right\}\exp(2\pi j\Delta f(t))\boldsymbol{H}_{\text{noise}}^H(t)] = 0$ because $E[\boldsymbol{H}_{\text{noise}}(t)] = 0$, and the noise is independent of other components. Also, $E[\boldsymbol{H}_{\text{vital}}(t)\boldsymbol{H}_{\text{fix}}^H] \simeq E[\boldsymbol{H}_{\text{fix}}\boldsymbol{H}_{\text{vital}}^H(t)] \simeq 0$ because we assume $E[\boldsymbol{H}_{\text{vital}}] = 0$, and $\boldsymbol{H}_{\text{vital}}(t)$ and $\boldsymbol{H}_{\text{fix}}$ are independent.

It is obvious that $\boldsymbol{H}_{\text{fix}}$ is dominant in the channel $\boldsymbol{H}(t)$ because it contains the direct path, and the largest eigenvalue in $\boldsymbol{R}_{M_R}$ corresponds to the path intensity of the $\boldsymbol{H}_{\text{fix}}$. Then, the eigenvalue decomposition is applied to $\boldsymbol{R}_{M_R}$ as follows,

$$
\boldsymbol{R}_{M_R} = \boldsymbol{U}_R\boldsymbol{D}_R\boldsymbol{U}_R^H,
\tag{2.9}
$$

$$
\boldsymbol{U}_R = [\boldsymbol{u}_{R1}, \boldsymbol{u}_{R2}, \ldots, \boldsymbol{u}_{RM_R}],
\tag{2.10}
$$

$$\boldsymbol{D}_R = \mathrm{diag}\,[\lambda_{R1}, \lambda_{R2}, \ldots, \lambda_{RM}], \tag{2.11}$$

where $\boldsymbol{U}_R$ is an eigenvector matrix, and $\boldsymbol{D}_R$ is a diagonal eigenvalue matrix, where $\lambda_{R1} \geq \lambda_{R2} \geq \ldots \geq \lambda_{RM}$. Similarly, the correlation matrix at the transmitter side is computed by

$$\begin{aligned}
\boldsymbol{R}_{M_T} =& E\big[\boldsymbol{H}\,(t)^H \boldsymbol{H}\,(t)\big] \\
\simeq& E\left[\boldsymbol{H}_{\mathrm{fix}}\boldsymbol{H}_{\mathrm{fix}}^H\right] + E\left[\boldsymbol{H}_{\mathrm{vital}}(t)\boldsymbol{H}_{\mathrm{vital}}^H(t)\right] \\
&+ E\left[\boldsymbol{H}_{\mathrm{noise}}(t)\boldsymbol{H}_{\mathrm{noise}}^H\,(t)\right],
\end{aligned} \tag{2.12}$$

and $\boldsymbol{R}_{M_T}$ is decomposed as,

$$\boldsymbol{R}_{M_T} = \boldsymbol{V}_T \boldsymbol{D}_T \boldsymbol{V}_T^H, \tag{2.13}$$

$$\boldsymbol{V}_T = [\boldsymbol{v}_{T1}, \boldsymbol{v}_{T2}, \ldots, \boldsymbol{v}_{TM_T}], \tag{2.14}$$

$$\boldsymbol{D}_T = \mathrm{diag}\,[\lambda_{T1}, \lambda_{T2}, \ldots, \lambda_{TM}]. \tag{2.15}$$

Because the 1st eigenvectors mainly represent the direct path as described above, $\boldsymbol{u}_{R1}$ and $\boldsymbol{v}_{T1}$ can retrieve the direct paht 's signal response as,

$$\Phi(t) = \boldsymbol{u}_{R1}^H \boldsymbol{H}(t)\boldsymbol{v}_{T1}. \tag{2.16}$$

Finally, by using $\phi(t)$, the frequency deviation $2\pi\Delta f(t)$ can be removed as,

$$\boldsymbol{H}_{\mathrm{cal}}(t) = \boldsymbol{H}(t)\Phi^{-1}(t). \tag{2.17}$$

At this time, a new time-variant channel $\boldsymbol{H}_{\mathrm{cal}}(t)$ without phase error is calculated.

2.3 Simulation

2.3.1 Simulation condition

Table 3.1 lists the simulation parameters assumed in this study. The number of the transmitting and receiving antennas is 8 at both sides. The distance between transmitter and receiver is 7 m, the antenna height is set to 1.0 m, and the element spacing for both transmitter and receiver arrays is 0.5 wavelength. The room is assumed to be 8×8 m. A zero-mean Gaussian noise matrix is added to the channel matrix to simulate a multipath environment. We assume the presence of a single living body, and the data of a total of 64 trials are collected. The vital sign channel with various frequency errors is calculated; the vital sign frequency range is set from 0.1 Hz to 5 Hz. In order to utilize the direct path, the direct path channel between the transmitter and receiver is also calculated. The total power $P_{vital} + P_{direct}$ is assumed to equal 1. Finally, the time-variant MIMO channel is computed by summing the vital sign, direct path, and noise components.

Table 2.1: Simulation condition

Number of Tx	8
Number of Rx	8
Element spacing d, [m]	0.5λ
Frequency used [GHz]	2.47125
Sampling frequency [Hz]	250
Height of antenna, h [m]	1.0
Observation time [s]	30
Number of targets	1
Frequency error [Hz]	$0 \sim 100$
Number of target positions	64
Vital sign frequency [Hz]	0.5
Extracted frequency range [Hz]	$f_1 = 0.1$ (lowest), $f_2 = 5.0$ (Highest)
Power ratio, $\dfrac{P_{vital}}{P_{direct}}$ [dB]	$-20 \sim 20$
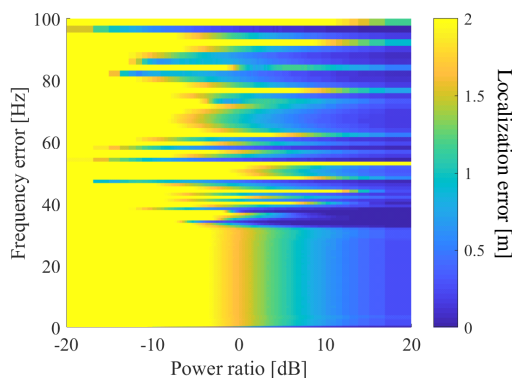
Figure 2.2: Localization error versus power ratio and frequency error (without phase correction).
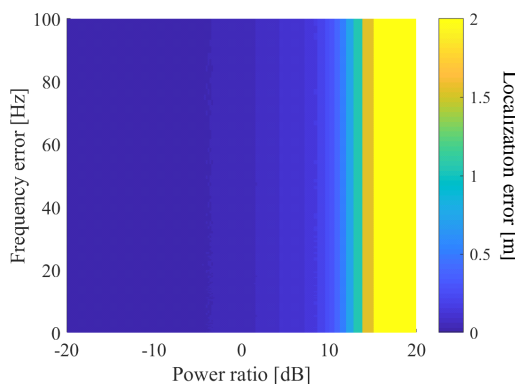
Figure 2.3: Localization error versus power ratio and frequency error (with phase correction).

2.3.2 Simulation results

Fig.2.2 shows localization error versus power ratio and frequency error. As shown in this figure, when the power of the vital sign is weak, and frequency error exists, the localization error is around 2 m, which

means the radar system is failing to detect the target location because there is no phase correction. As the power of the vital sign increases, the localization error is reduced.

Fig.2.3 plots localization error versus power ratio and frequency error when the proposed phase correction method is applied to the channel. As shown in this figure, even when the power of the vital sign is weak and frequency error exists, the proposed method can successfully counter the frequency error, and localization error is almost 0 m. However, the proposed method does not work when the power of the vital sign exceeds the power of the direct path, even though this situation does not happen in a natural environment. This is because this method tries to synchronize with the dominant path between the transmitter and receiver. When the power of the vital sign is stronger than the direct path, this MIMO system eliminates vital signs in this condition, and localization error becomes significant. This means the proposed method can eliminate the phase error successfully within a feasible range.

2.4   Measurement

2.4.1   Measurement conditions

Table 2.2: Experiment condition

Antenna element	Horizontal patch antenna
Number of Tx	8
Number of Rx	8
Element spacing, d [m]	0.5λ
Angle of the antennas	45
Frequency used [GHz]	2.47125
Sampling frequency [Hz]	250
Antenna height, h [m]	1
Observation time [s]	30
Number of targets	$1 \sim 6$
Distance between targets [m]	2
Number of measurement points	30
Extracted frequency range [Hz]	$f_1 = 0.1$ (lowest), $f_2 = 5.0$ (highest)

Figure 2.8(a) and Figure 2.8(b) shows the photos of the antenna used in the experiment. In this experiment, the distance between transmitter and receiver is 8 m, and the direction of the transmitter and receiver is 45 degrees into the monitoring area so that the whole space can be covered by the electromagnetic waves. The height of the antenna was set to 1.0 m, and the element spacing for both transmitter and receiver was 0.5 wavelength.

Figure 2.5 shows the system overview of this experiment. The signal generators (SGs) provide a continuous wave (CW) signal of 2.47125 GHz at both the transmitter and receiver sides. The generated
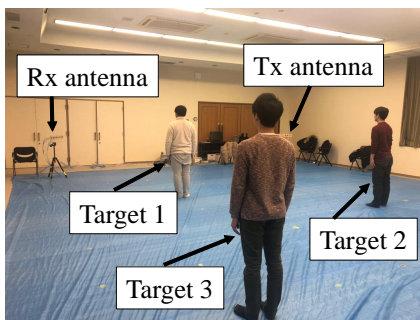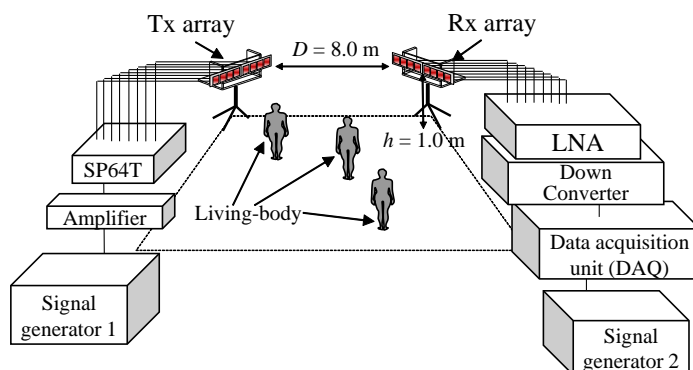
Figure 2.4: Measurement setup.

Figure 2.5: System overview. In this experiment, in order to emulate both synchronized and unsynchronized condition, independent signal generators are used at the transmitter and receiver sides.
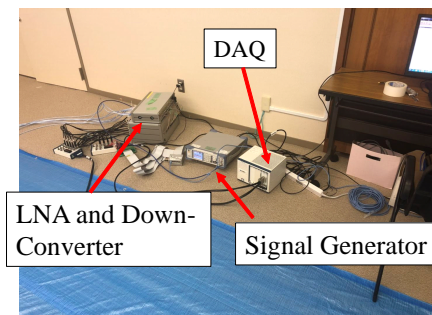

Figure 2.6: Measurement environment.

signal at SG1 went through ATT (Attenuator) and the transmitting amplifier to control the transmitted power. A single-pole 64 throw (SP64T) is used to switch the signal to all transmitter antennas. In this experiment, the SG1 output was set at 15 dBm, the ATT was set at 20 dB, and the gain of the transmitting amplifier is 24 dB. The power at the transmitting antenna port was at 8.4 dBm because the power is attenuated by the cables and SP64T.

At the receiver side, the received signals are input to a down-converter (DC) unit by way of low-
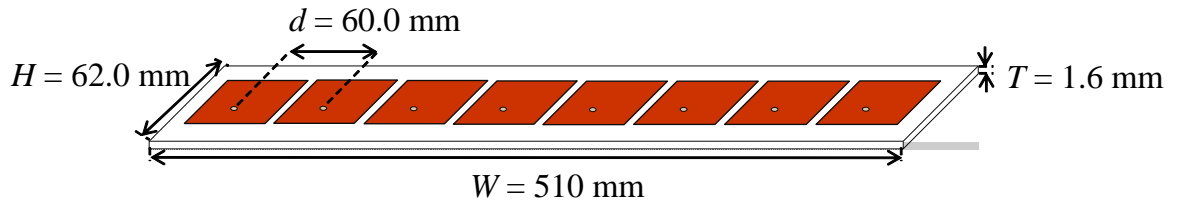
Figure 2.7: Overview of microstrip antenna array

(a) Tx

(b) Rx
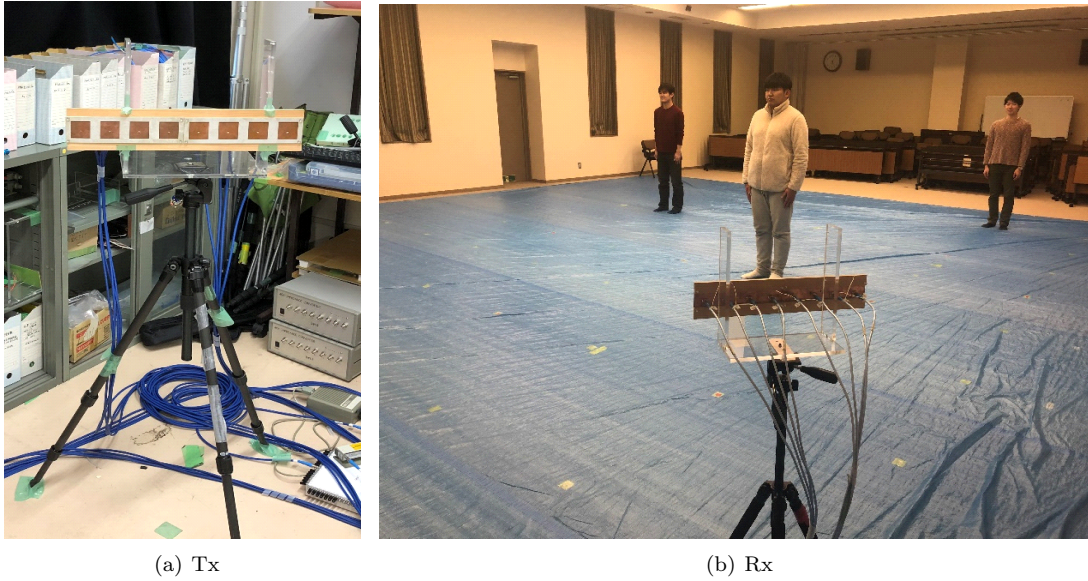
Figure 2.8: Photos of antenna used in the experiment

noise amplifier (LNA). Then the down-converted baseband signals (I_1,Q_1, I_8,Q_8) are digitized and recorded by data-acquisition unit (DAQ). Figure 2.9 shows a photo of the receiver system used in the measurement. The signals output from the receiver antennas are input to the DC via an LNA with a gain of 40 dB.

In order to emulate the unsynchronized condition, as shown in Fig. 2.10, there were 2 independent SGs used for the transmitter and receiver sides.
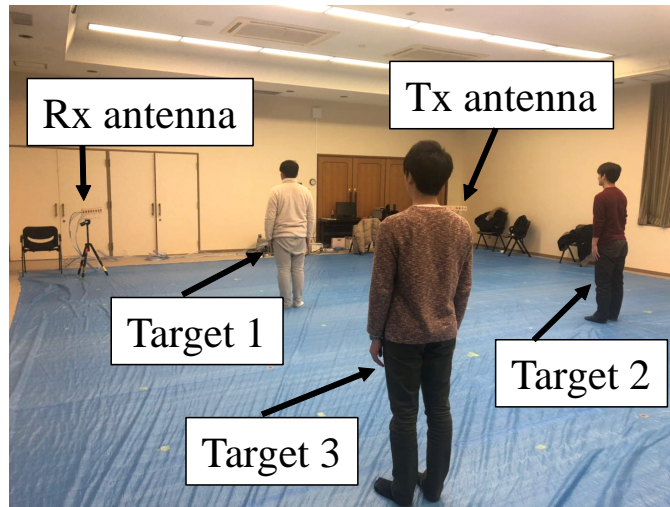
Figure 2.9: Instruments of the experiment
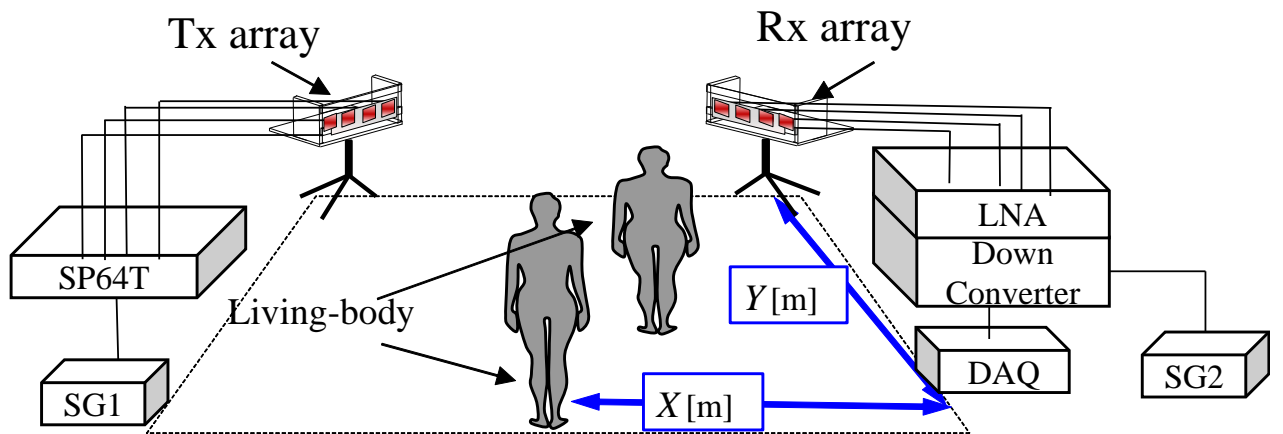
Figure 2.10: System overview including targets

2.4.2　Experimental environment

Table 3.1 shows the more detailed condition of the measurement and Fig. 2.11 shows the measurement environment. The measurement was carried out in an indoor multipath-rich environment, and the size of the room was 8 by 8 meters. Two different kinds of experiments, i.e. synchronized and unsynchronized were tested. In each trail, the number of the targets were tested from one to six. Each of the target were stood in 30 different random measurement points. By considering the accuracy of the experiment, the distance between the two targets were set to be greater than or equal to 2 m. The fluctuating components from 0.3 Hz to 5 Hz were extracted in order to eliminate the unwanted components and only the fluctuation created by vital signs, i.e. heartbeat and respiration, were observed.

In this verse, the result of the single-target detection with three conditions as follows. The first one is an ideal case, where the transmitter and receiver are fully synchronized. The second one is a conventional case, where no phase correction is performed while the transmitter and receiver frequencies are not synchronized. The third one used a proposed phase correction method, where the transmitter and receiver frequencies are not synchronized.

Figure 2.12 shows the result of the temporal response of the channel with (a) synchronization (ideal condition) and (b) conventional method (unsynchronized condition without any phase correction process). In an ideal condition, we can see the vital sign component as a smooth fluctuation. The channel information can be observed very clearly. However, when it turns to the conventional method, channel of the human-body component is failed to detect and completely mixed with the other interruption.

Figure 2.13 shows the frequency spectrum with (a) synchronization (ideal situation) and (b) conventional method (unsynchronized condition without any phase correction process). The frequency response of the channel caused by human-body motion can be clearly observed in ideal condition. However, because of the frequency offset causes the serious phase error in the conventional method, the vital sign failed to be detected.

Figure 2.14 shows the examples of the single target localization result of the MUSIC spectrum in (a) synchronized and (b) conventional condition. The pink circles represent the actual positions and black crosses represent the estimated positions, the standing position of this single target was (4, 5) m. As shown in this figure, the estimated location appears near the actual location of the target in synchronized one. In conventional method, it failed to estimate because the phase error caused serious degradation in detection performance.

As we mentioned in the chapter 2, by applying the frequency offset elimination technique, phase

error can be eliminated theoretically. In this discussion, the experimental result of the unsynchronized condition with phase error correction will be presented and compared with the ideal situation. Figure 2.15 shows temporal response of the channel with proposed method. We can see the vital sign component with a smooth fluctuation after the phase error correction. Figure 2.16 shows the frequency spectrum with proposed method. It is shown that the Doppler shift due to human-body motion can be clearly observed by our proposed method.

Figure 2.17 shows the examples of the single target localization result of the MUSIC spectrum. As shown in this result, the peak value of the spectrum appear near the actual location of the target. It means that the proposed method works well as the synchronized one in this case.

Figure 2.18 shows the Cumulative-Distribution-Function (CDF) of distance error by comparing three different ways to estimate single target position. The result shows that 50-percentile localization error was 0.3 m, 4 m , 0.7 m for ideally synchronized case (synchronized), conventional method (unsynchronized), proposed method (proposed). It indicates that in unsynchronized condition, the 50 percentile of distance error was decreased from 4.0 m to 0.7 m, which means our proposed method can estimate the single target's locations with high accuracy.

Although our proposed works well in single target localization, as we mentioned in chapter 2, compared with single, multiple targets detection is more complicated. The performance of the multiple targets localization with the proposed method is needed. In this experiment, the number of the targets was tested from two to six. Each of the target was stood in 30 different random measurement points, the distance between the two targets was set to be greater than or equal to 2 m. The results of the multiple targets detection with ideal case, conventional method, and proposed method were shown and discussed as below.

Figures 2.28 show the examples of the multiple target localization result of the MUSIC spectrum in synchronized (left side) and conventional situation (right side). The number of the target was tested from 2 to 6. The pink circles represent the actual positions and black crosses represent the estimated positions, the standing position of two targets was (0, 5) m and (6, 5) m, positions of three targets was (0, 3) m, (0, 7) m and (4, 7) m, positions of four targets was (0, 5) m, (2, 3)m , (4, 1) m and (6, 5) m, positions of five targets was (0, 5) m, (4, 3) m, (4, 1) m, (4, 5) m and (6, 5) m, positions of six targets was (0, 1) m, (2, 1) m, (2, 3) m, (4, 5) m, (6, 7) m and (6, 5) m. As shown in these figures, most of the estimated locations appear near the actual locations of the targets in synchronized one. In the conventional method, as well as the single target's result, most of the positions failed to be estimated because the phase error caused serious degradation in detection performance.
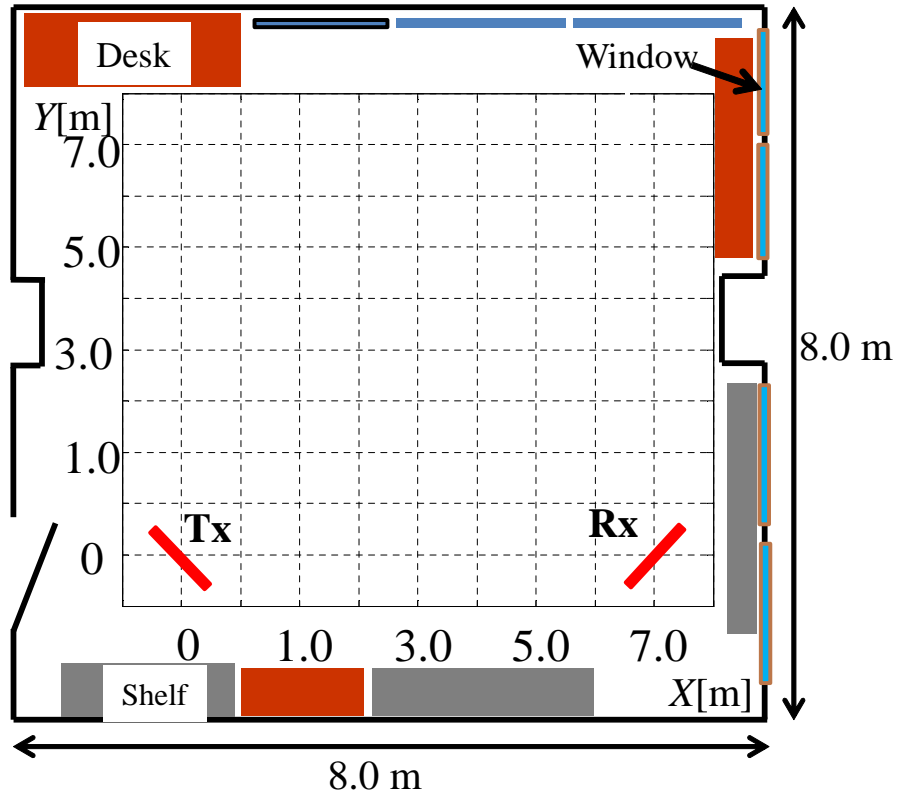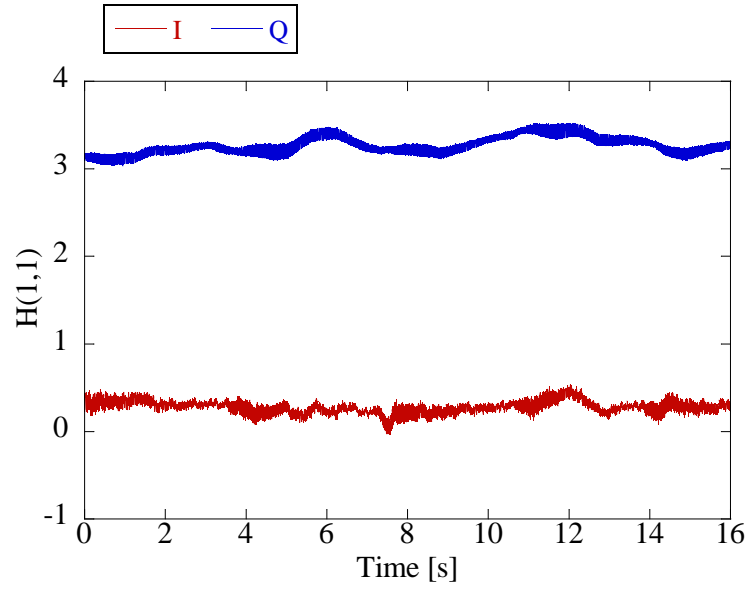
(a) All scenes of the experiment

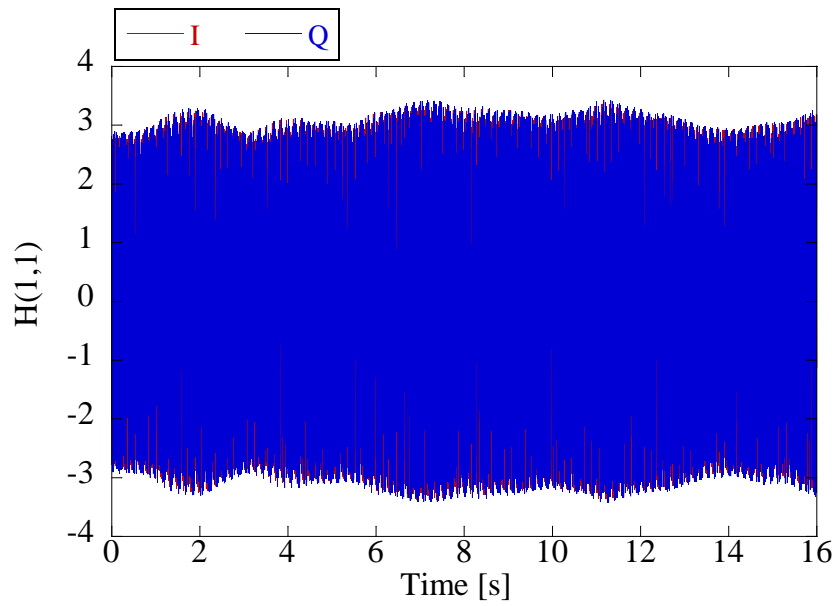(b) Photograph of the back side

(c) Photograph of the front side

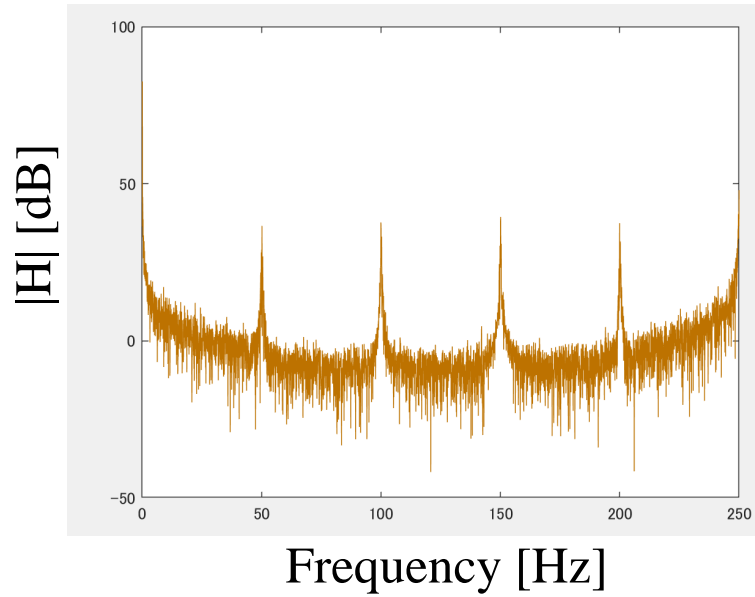Figure 2.11: Measurement environment
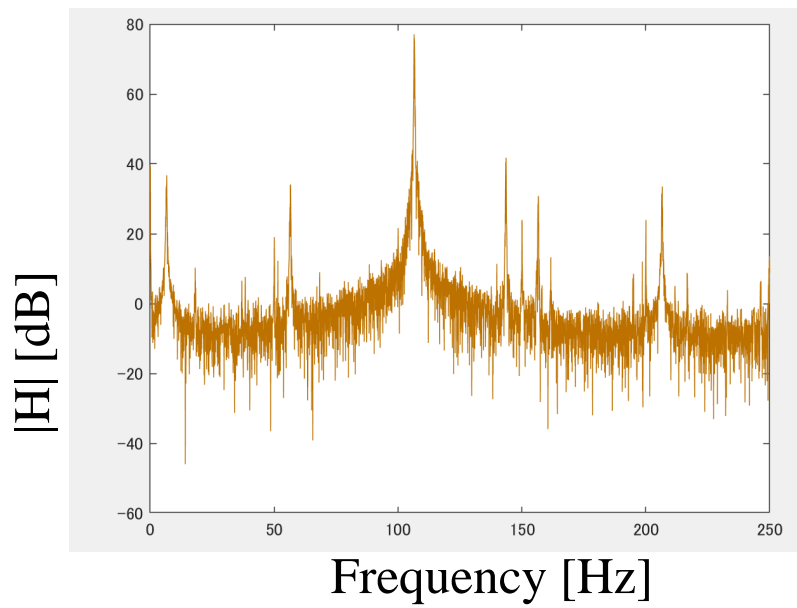
(a) Synchronized (ideal situation)

(b) Unsynchronized (conventional method)

Figure 2.12: Temporal response of the channel

(a) Synchronization (ideal situation)

(b) Unsynchronized (conventional method)
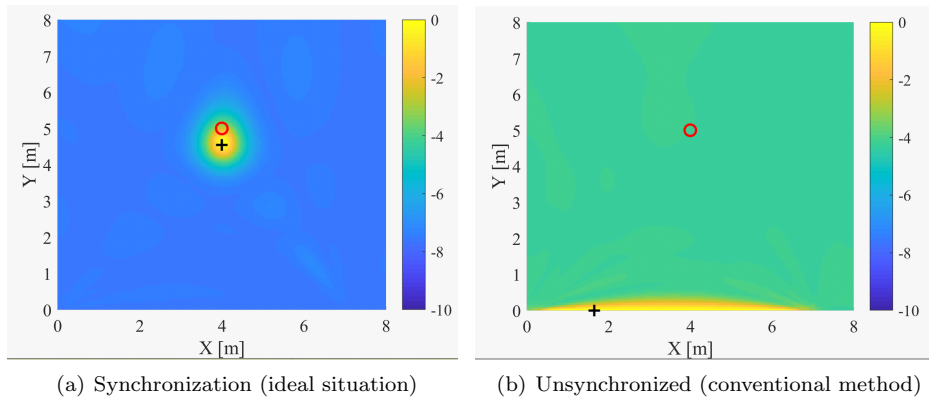
Figure 2.13: Frequency spectrum

(a) Synchronization (ideal situation)

(b) Unsynchronized (conventional method)

Figure 2.14: Example of the single target localization result
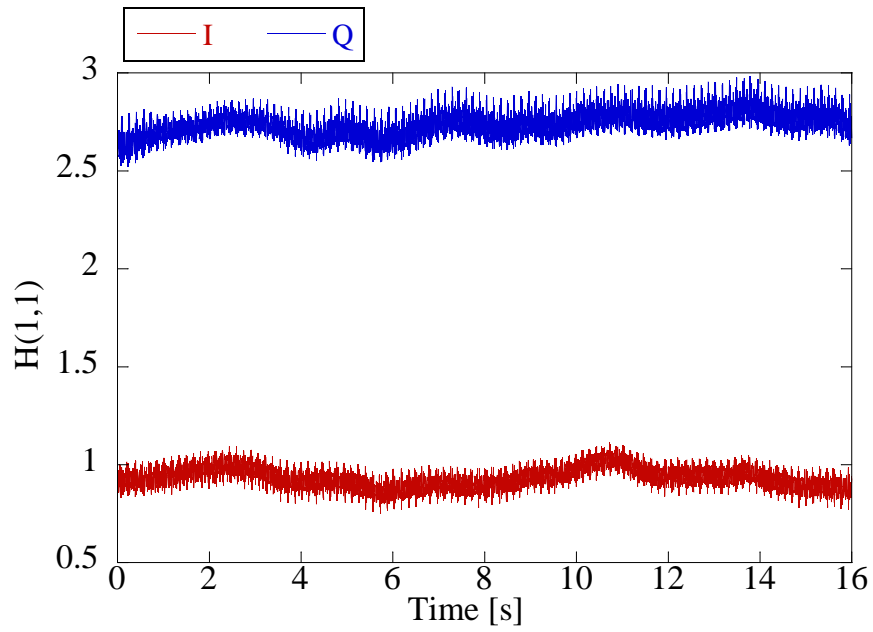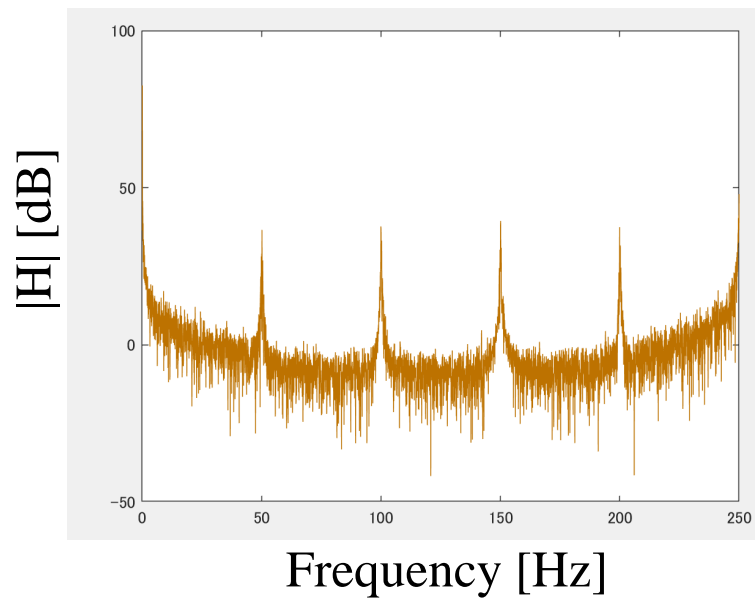

Figure 2.15: Temporal response of the channel

Figure 2.16: Frequency spectrum

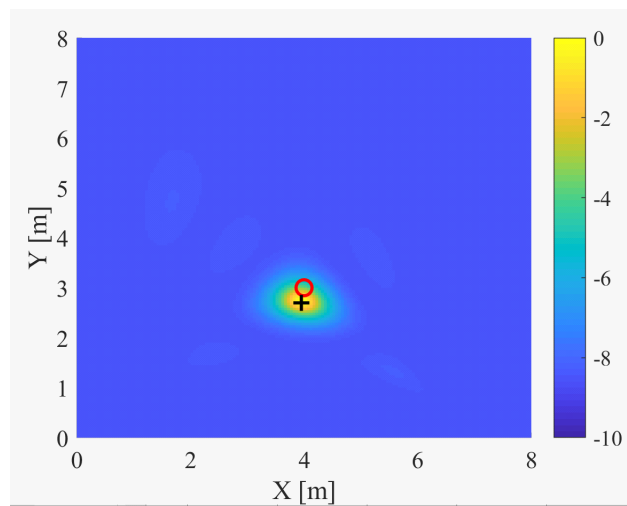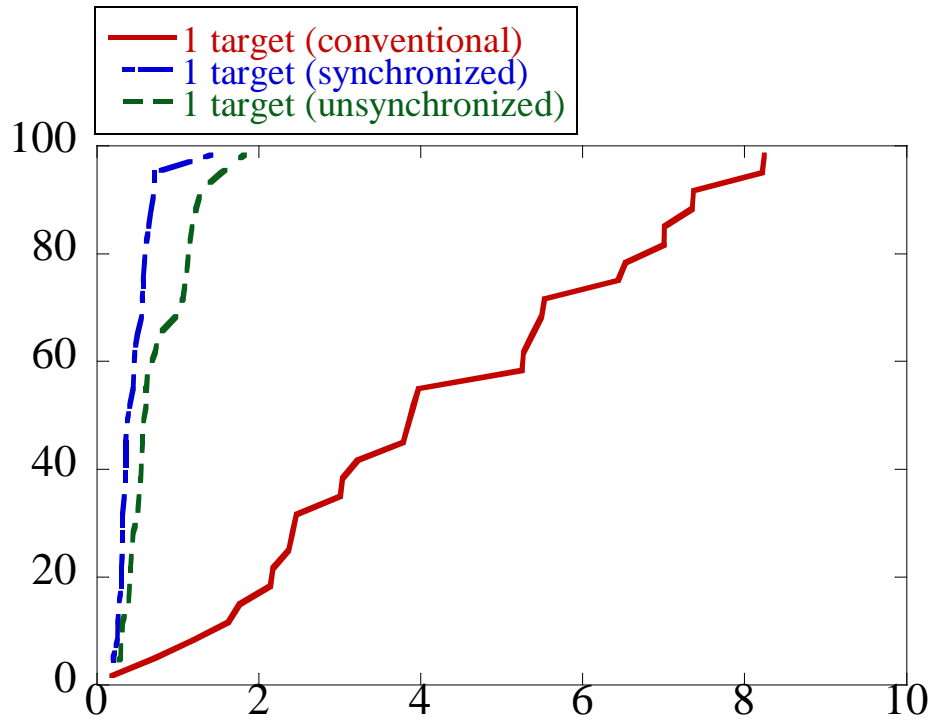Figure 2.17: Example of the single target localization result

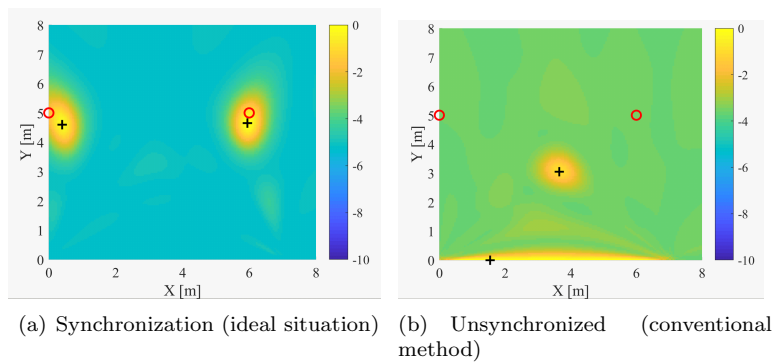Figure 2.18: CDF of the localization error with single target

(a) Synchronization (ideal situation)

(b) Unsynchronized (conventional method)

Figure 2.19: MUSIC spectrum examples of the 2 targets localization result

(a) Synchronization (ideal situation) (b) Unsynchronized (conventional method)
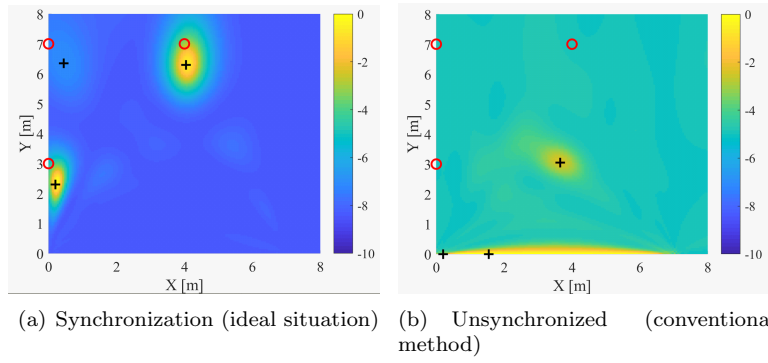
Figure 2.20: MUSIC spectrum examples of the 3 targets localization result

(a) Synchronization (ideal situation) (b) Unsynchronized (conventional method)
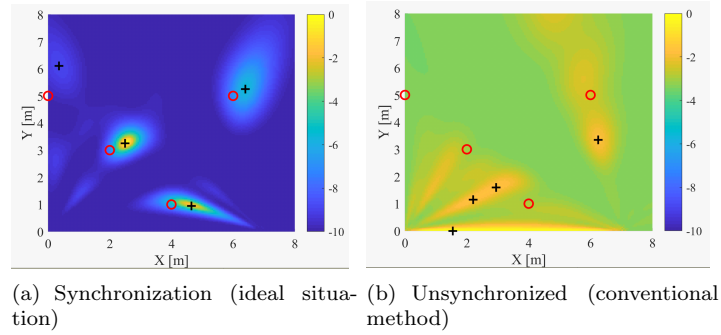
Figure 2.21: MUSIC spectrum examples of the 4 targets localization result

(a) Synchronization (ideal situation) (b) Unsynchronized (conventional method)
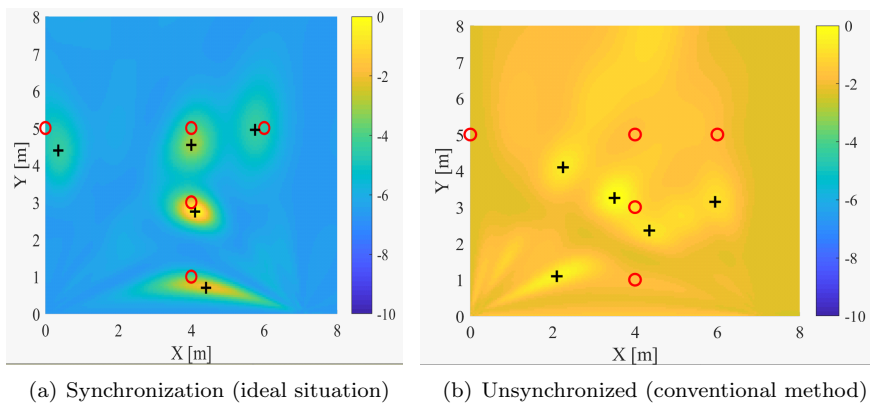
Figure 2.22: MUSIC spectrum examples of the 5 targets localization result

(a) Synchronization (ideal situation) (b) Unsynchronized (conventional method)
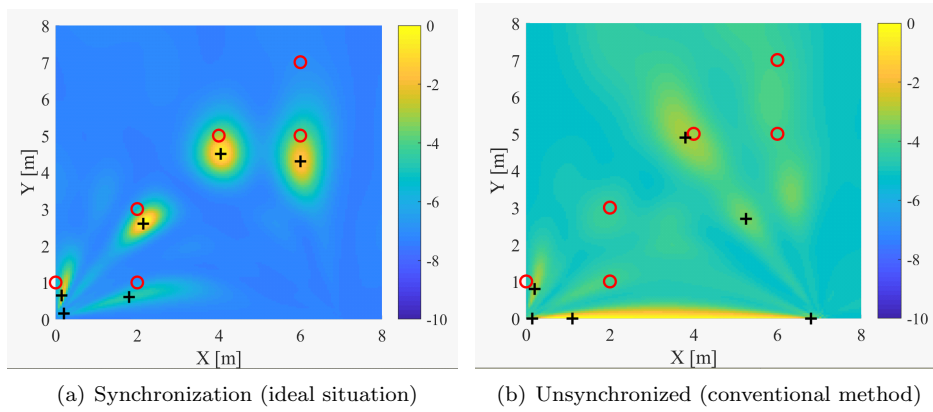
Figure 2.23: MUSIC spectrum examples of the 6 targets localization result

By applying the frequency offset elimination technique, Figs. 2.28 show the examples of the multiple targets localization result of the MUSIC spectrum in the unsynchronized situation (proposed method) and compared with the synchronized (ideal condition). In order to better comparison, the standing positions were same in both cases. As shown in these figures, in unsynchronized condition, when the number of the targets were two and three, the peak values of the spectrum appear near the actual locations of the targets and are successfully estimated. When the number of the targets were four, five and six, one of them was frequently failed to be recognized in each trail due to the interaction of this radar's performance and the propagation environment, and yet proposed method can estimate the locations of the rest of the targets accurately.
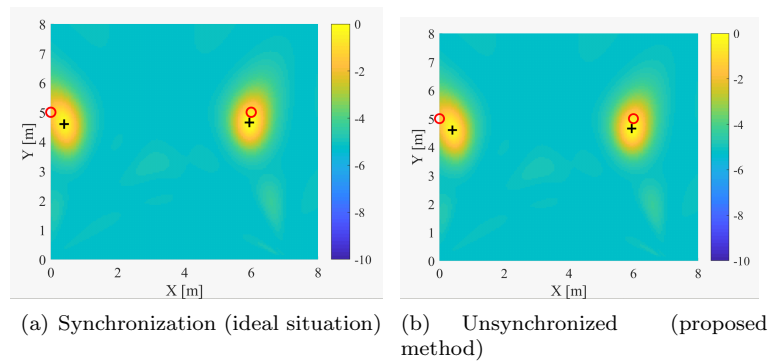

(a) Synchronization (ideal situation)   (b)   Unsynchronized   (proposed method)

Figure 2.24: Example of the 2 targets localization result

(a) Synchronization (ideal situation) (b) Unsynchronized (proposed method)
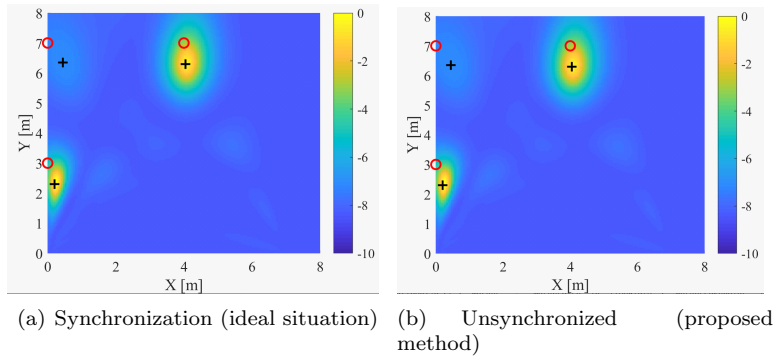
Figure 2.25: Example of the 3 targets localization result

(a) Synchronization (ideal situation) (b) Unsynchronized (proposed method)
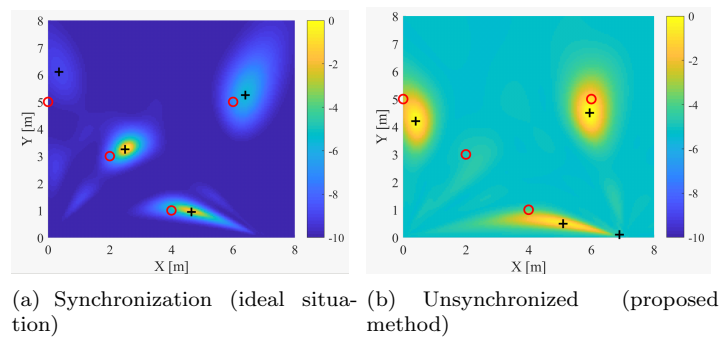
Figure 2.26: Example of the 4 targets localization result

(a) Synchronization (ideal situation)   (b) Unsynchronized (proposed method)
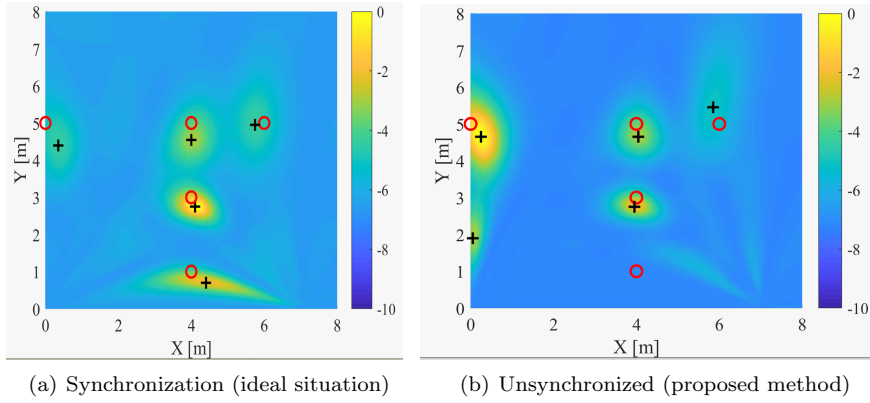
Figure 2.27: Example of the 5 targets localization result

(a) Synchronization (ideal situation)   (b) Unsynchronized (proposed method)
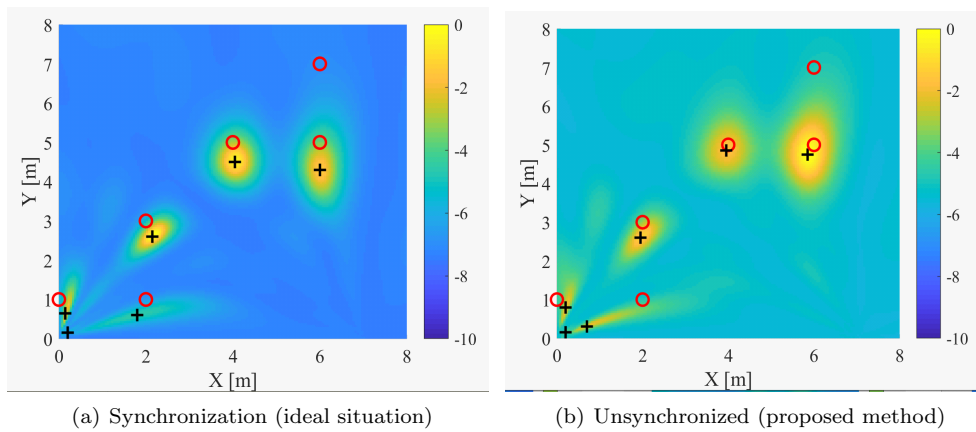
Figure 2.28: Example of the 6 targets localization result

Figures 2.29 shows the CDF of distance error with various numbers of the targets. As shown in this figure, the value of 50% of location errors were 0.80 m, 0.95 m, 1.12 m, 1.96 m and 1.02 m for 2∼6 targets in unsynchronized condition. The results indicated that proposed method accurately estimates target location in an acceptable accuracy even when the number of the targets were up to six.

Figure 2.29: CDF of the conventional method, synchronized and proposed method with multiple targets

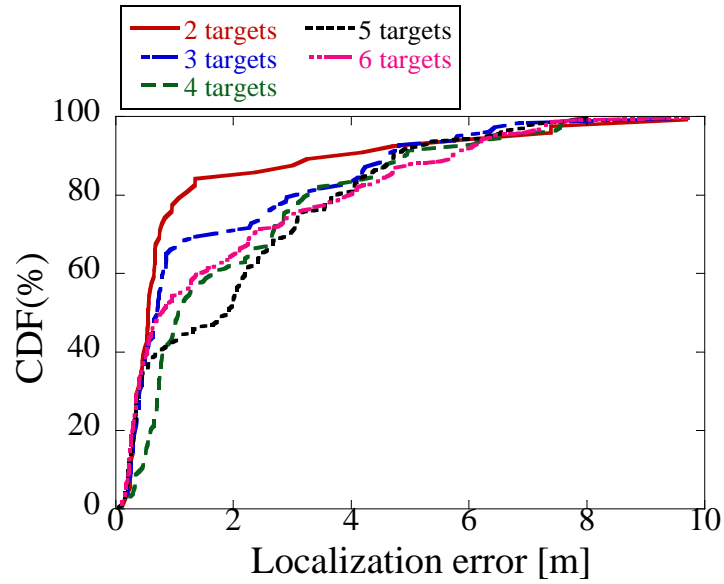Figures 2.30 shows the result of the unsynchronized localization errors at 50%, 75% and 90% corresponding to number of the target from one to six. As shown in this figure, the localization error at 50% was 0.70 m, 0.80 m, 0.95 m, 1.12 m, 1.96 m and 1.02 m at the number of the targets is varied from 1 to 6, and fluctuation was relatively flat. We can see that the 50% of localization error is increasing when the number of the target is from one to five because of the limitation of the degree of freedom in the MIMO array. But when it turns to 6-target, the distance error is going down again. One of the reasons is that the distribution of the target's position. When there are too many targets that exist randomly, the peak value of MUSIC spectrum is accidentally shown up near to the actual position which causes the line down. The value of 75% of localization errors was 1.12 m, 1.05 m, 3.15 m, 3.96 m, 4.04 m, and 4.12 m for 1∼6 targets. We can see that when the number of the target is increasing, from 3-target, the value is significantly changed and tend to increase. These results also indicated that the tendency of the localization error is different at a different percentage. Clearly, the result of this figure reveals that our MIMO radar works well even the number of the targets are up to six in this indoor environment.
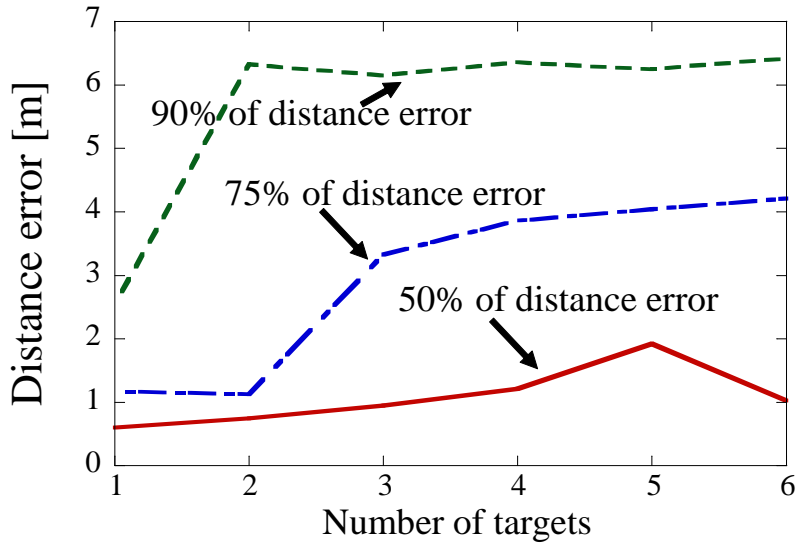

Figure 2.30: Localization error versus the number of targets

To better demonstrate the effectiveness of our radar system, the following figures show the CDF of the localization error by comparing three different ways to 2∼6 targets position.

Fig.2.31 shows the localization error with the 2 targets. The result shows that 50-percentile local-

ization error was 0.50 m, 3.66 m, 0.80 m for conventional method (synchronized), conventional method (unsynchronized), proposed method (unsynchronized). It indicates that in unsynchronized condition, the 50 percentile of distance error was decreased from 3.66 m to 0.80 m,

Fig.2.32 shows the localization error with the 3 and 4 targets. The result (a) shows that 50-percentile localization error in 3 targets was 0.61 m, 3.87 m , 0.95 m and (b) shows localization error in 4 targets was 0.87 m, 3.84m 1.12 m for the conventional method (synchronized), conventional method (unsynchronized), proposed method (unsynchronized). It is seen that the proposed method can work fairly as in the synchronized condition even with a small degradation in the localization accuracy.

Fig.2.33 shows the localization error with the 5 and 6 targets. The result (a) shows that 50-percentile localization error in 5 targets was 1.95 m, 3.83 m , 1.96 m and (b) shows localization error in 6 targets was 0.92 m, 3.76 m 1.02 m for the conventional method (synchronized), conventional method (unsynchronized), proposed method (unsynchronized). It is confirmed that the proposed method can identify the location of the multiple targets (up to six) with an accuracy as high as the synchronized one.

Figure 2.31: CDFs of synchronized, unsynchronized and conventional localization error with 2 targets.

(a) CDFs of synchronized, unsynchronized and conventional localization error with 3 targets.

(b) CDFs of synchronized, unsynchronized and conventional localization error with 4 targets.

Figure 2.32: localization error with the 3 and 4 targets

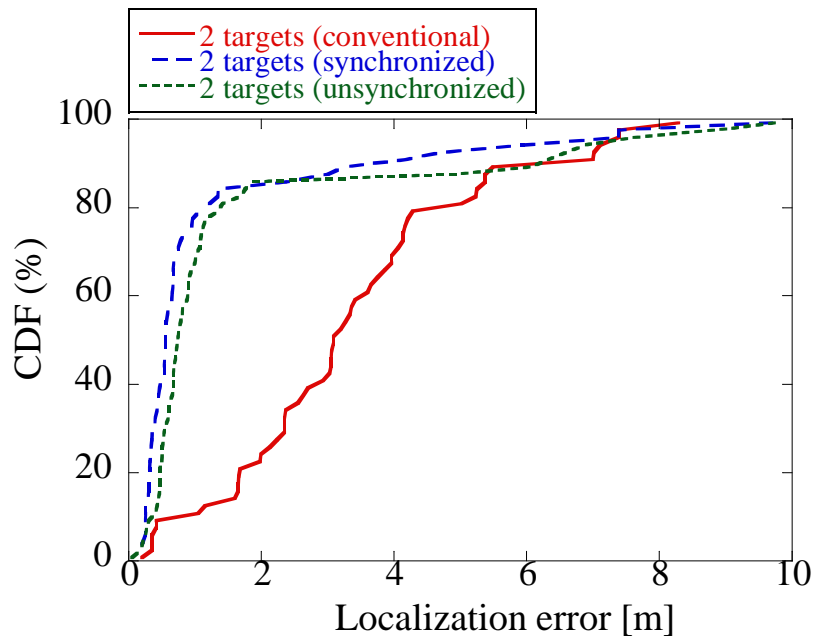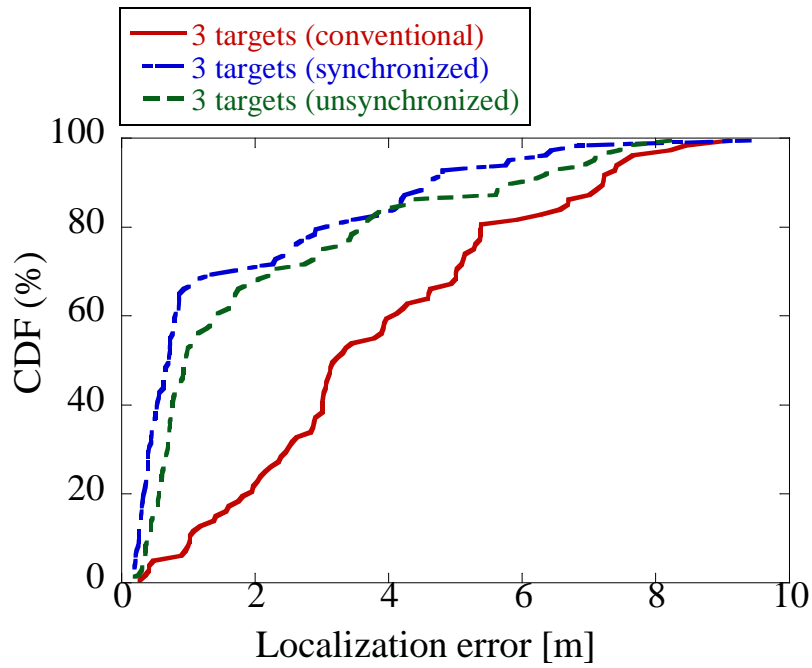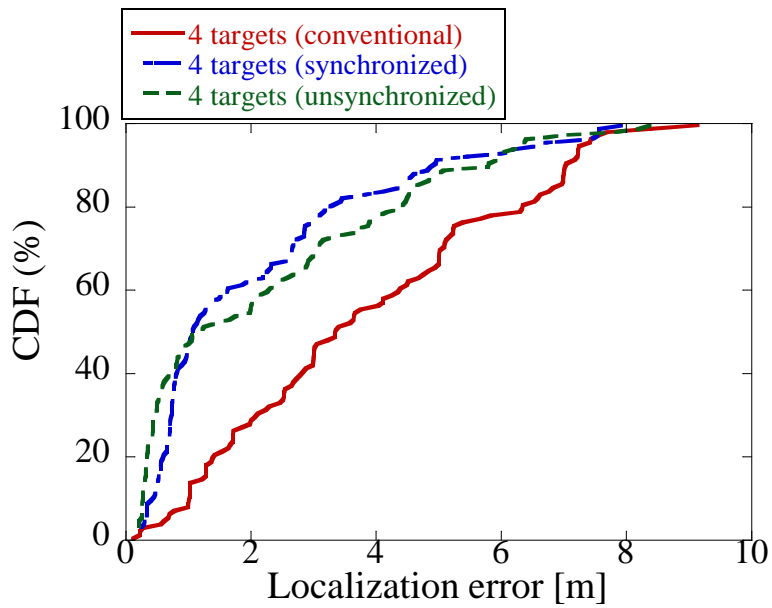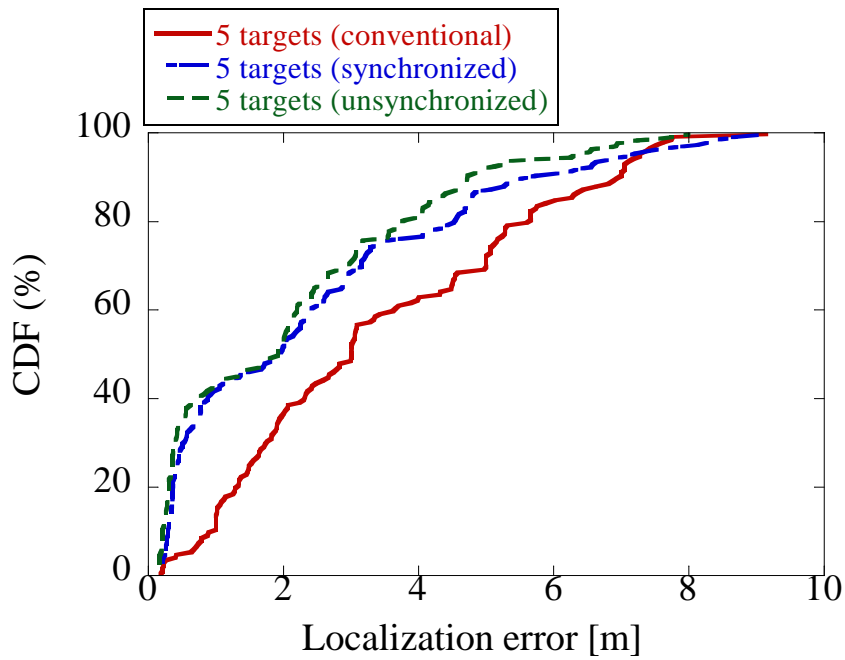(a) CDFs of synchronized, unsynchronized and conventional localization error with 5 targets.

(b) CDFs of synchronized, unsynchronized and conventional localization error with 6 targets.
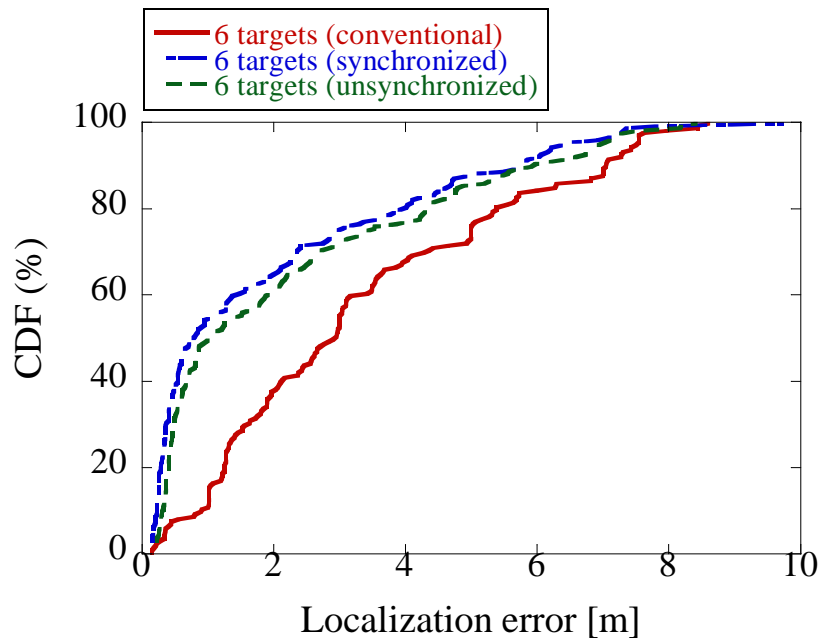
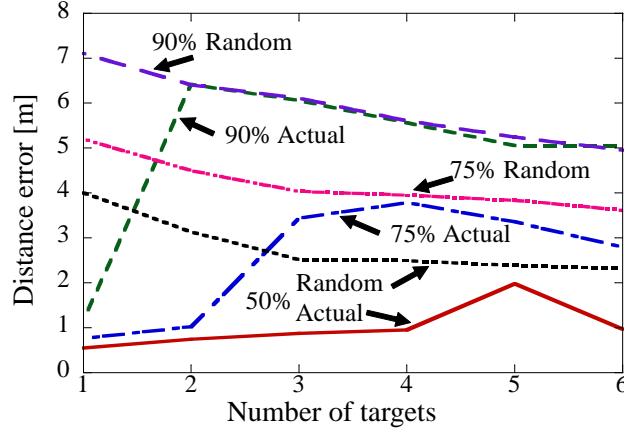Figure 2.33: localization error with the 5 and 6 targets

Figure 2.34: Localization error versus the number of targets.

Fig.2.34 shows the 50%, 75%, and 90% localization errors for the proposed method and random positions versus the number of targets. The random positions are added to this result where the targets appear randomly and irregular at the same condition, which is the worst condition. As shown in this figure, the localization errors of 50% for the proposed method were 0.55 m, 0.74 m, 0.87 m, 0.95 m, 1.98 m, and 0.96 m for the number of targets from 1 to 6; the fluctuation was relatively minor. We can see that the 50% localization error increases when the number of targets increases from one to five because of the limitation of the DOA/DOD resolutions. In the 6-target case, however, the distance error is decreased. One of the reasons is the distribution of target positions. When too many targets are randomly placed, the peak value of MUSIC spectrum accidentally shows up near the actual position, which decreases the location error. The values of 75% localization errors for the proposed method were 0.75 m, 1.01 m, 3.43 m, 3.78 m, 3.35 m, and 2.80 m for 1 to 6 targets. As the number of the target increases, the value changes significantly and tends to increase from 3-targets. With random positioning, the 50%, 75%, and 90% localization errors also tend to decrease as target number increases. As we described above, when there are too many targets, the error appears to be bounded because the incorrectly estimated positions eventually come close to the actual position due to the densely distributed targets. By looking at the 90% results, the estimated results become close to random if we have multiple targets, but this is the worst case. The 50% result shows that our radar can detect up to 4 targets because the estimation error is less than half that shown by the random results. These results also indicate that the localization error exhibits different characteristics at different percentages.

37

Clearly, the result of this figure reveals that our MIMO radar can work fairly well even with up to 6 targets in this indoor environment.

2.5 Conclusion

In this chapter, we presented and experimentallyevaluatede a frequency error elimination technique suitable for unsynchronized bistatic MIMO radar for human-body detection. First, a mathematical expression of human body localization using bistatic MIMO radar is presented. Then the direct path is used to eliminate the phase error created by the frequency difference between the transmitter and receiver. A new Doppler-shifted component of the MIMO channel without phase error is derived, and the locations of the multiple targets are calculated by the 2-dimensional MUSIC method. Next, the results of simulations that examine frequency error versus power ratios are discussed to illustrate the effectiveness of the proposed method. An experiment is carried out in an indoor multipath-rich environment. To emulate the unsynchronized condition, the transmitter and receiver use independent SGs. One to six targets are tested. The experiments demonstrate that our unsynchronized radar system can identify the locations of multiple targets with high accuracy.

Chapter 3

SIMO antenna array based indoor localization technique of multiple human-bodies using roundtrip channels

In previous section, we proposed a frequency error elimination technique for unsynchronized bistatic CW-MIMO radar for multiple human-body detections. However, this system requires the use of multiple antennas at both the transmitting and receiving stations, which results in the need for costly additional hardware at both ends. Therefore, in order to be more budget-friendly, in this section, we introduce a SIMO antenna array based indoor localization technique of multiple human-bodies using roundtrip channels.

3.1 Technical issues in COTS-based SIMO radar

In the design of SIMO radar systems, there is a prevalent utilization of commercially available COTS components. These COTS components, while advantageous in terms of cost-effectiveness and facilitating a more streamlined development process, also introduce certain technical challenges that warrant consideration. Firstly, it's crucial to note that SIMO systems might be limited in their spatial resolution capabilities when juxtaposed with their full-MIMO counterparts, thereby potentially affecting their precision in estimating target positions. Secondly, despite the suitability of COTS components for SIMO radar systems, the inherent limitations in the accuracy of the local oscillator can lead to frequency errors in both the transmitter and receiver, consequently impacting the radar's localization abilities. This discrepancy might pose a notable hurdle in ensuring precise target localization. Thirdly, and notably, the challenge intensifies in scenarios involving the localization of multiple targets, as the
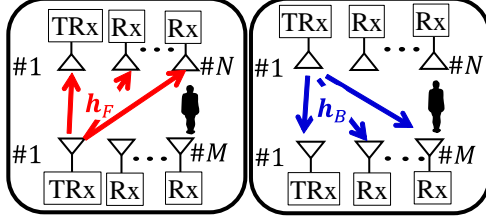
Figure 3.1: System framework.

amalgamated impact of the previously discussed limitations significantly compounds the complexities in accurately pinpointing and tracking more than one target.

3.2 Method of frequency adjustment and target positioning using roundtrip SIMO channel

Fig.3.1 shows the system framework of this study. We assumed that there are two stations (transmitter and receiver stations); each has multiple antennas, where only a single antenna can transmit and receive, and the other antennas can only receive. Forward $N \times 1$ SIMO channel $\boldsymbol{h}_F$ and backward $M \times 1$ SIMO channel $\boldsymbol{h}_B$ were defined. First, we analyzed the frequency difference between forward and backward transmissions. Subsequently, a phase adjustment and elimination technique was applied to the merged channel. Living-body positioning relying only on SIMO channels was then performed.

3.2.1 Method of phase adjustment

The phase error owing to the limitation of the clock accuracy between the two stations strongly affects the localization accuracy. This section discusses the frequency offset in the roundtrip channels and proposes a phase-adjustment technique.

As shown Fig.3.1 (a) and (b), forward $N \times 1$ SIMO channel $\boldsymbol{h}_F$ and backward $M \times 1$ SIMO channel $\boldsymbol{h}_B$ are defined as,

$$\boldsymbol{h}_F(t) = [h_{F11}(t), \ldots, h_{F1N}(t)]^T, \tag{3.1}$$

$$\boldsymbol{h}_B(t) = [h_{B11}(t), \ldots, h_{BM1}(t)]^T, \tag{3.2}$$

respectively, where $\{\cdot\}^T$ represents the transposition, h_{ij} is the complex channel response from transmitter j to receiver i, and t represents the time of the channel observation. Note that the forward and backward transmission durations are nearly identical because of the slower rate of vital sign changes compared with the switching of observations between the forward and backward channels. As a result, the duration t for the forward and backward channels are similar. Here, h_{F11} and h_{B11} ideally have the

same value because they share the same antenna element. However, their phases do not agree because of the clock differences. Assume that the frequencies of a specific channel in the transmitter and receiver stations are f_1 and f_2, respectively. The transmitter and receiver have individual oscillators, and their frequencies are inherently different ($f_1 \neq f_2$) owing to the limitation of clock accuracy. Hence, the frequency deviation between the two oscillators Δf is defined as follows:

$$\Delta f = f_1 - f_2. \tag{3.3}$$

The differential angular frequency can be introduced as

$$\Delta \omega = 2\pi \left(f_1 - f_2 \right), \tag{3.4}$$

Subsequently, the forward $N \times 1$ SIMO channel $\boldsymbol{h}_F$ with a phase difference is expressed as

$$\boldsymbol{h}_F(t) = [h_{F11}(t), \ldots, h_{F1N}(t)]^T \exp(j\Delta\omega t). \tag{3.5}$$

The backward $M \times 1$ SIMO channel $\boldsymbol{h}_B$ with a phase difference is expressed as

$$\boldsymbol{h}_B(t) = [h_{B11}(t), \ldots, h_{BM1}(t)]^T \exp(-j\Delta\omega t). \tag{3.6}$$

The first element of $\boldsymbol{h}_F$ and $\boldsymbol{h}_B$ are expressed as

$$h_{F11}(t) = h_{11} \exp(j\Delta\omega t), \tag{3.7}$$

$$h_{B11}(t) = h_{11} \exp(-j\Delta\omega t), \tag{3.8}$$

respectively. Here, $\boldsymbol{h}_F$ and $\boldsymbol{h}_B$ cannot be merged because h_{F11} and h_{B11} have different phase errors. Because the observed phase rotations of the forward and backward channels are opposite, the phase error A_{FB} of forward channel $\boldsymbol{h}_F$ can be adjusted as follows:

$$
\begin{aligned}
A_{FB} &= \exp\left(j\frac{1}{2} \angle \frac{h_{B11}}{h_{F11}} \right) \\
&= \exp\left(j\frac{1}{2} \angle \frac{h_{11} \exp(-j\Delta\omega t)}{h_{11} \exp(j\Delta\omega t)} \right) \\
&= \exp\left(j\frac{1}{2} \angle \exp(-2j\Delta\omega t) \right) \\
&= \exp(-j\Delta\omega t).
\end{aligned}
\tag{3.9}
$$

Finally, phase error can be eliminated for both channels using the expression below:

$$\boldsymbol{h}'_F(t) = \boldsymbol{h}_F A_{FB} = [h'_{F11}, \ldots, h'_{F1N}]^T, \tag{3.10}$$

$$\boldsymbol{h}'_B(t) = \frac{\boldsymbol{h}_B}{A_{FB}} = [h'_{B11}, \ldots, h'_{BM1}]^T. \tag{3.11}$$

3.2.2 Target positioning using roundtrip SIMO channel

MIMO-based CW-radar for target detection, where DoD and DoA information are used, has been widely studied because it is known to provide good accuracy. In contrast, a narrowband SIMO radar only has the capability of DoA finding and is incapable of localizing the living body position owing to insufficient spatial information. In this section, we introduce a living-body positioning method that relies only on SIMO channels. This method combines roundtrip SIMO channels to estimate two DoDs bidirectionally to jointly localize the target position.

After the phase adjustment, by simply combining the two SIMO channels, we obtain a merged $M + N - 1$ SIMO channel as

$$\boldsymbol{h}'(t) = [h'_{B11}, \ldots, h'_{BM1}, h'_{F12}, \cdots h'_{F1N}]^T. \tag{3.12}$$

Subsequently, to exclude certain unwanted paths and extract only the vital signs, this channel is Fourier-transformed to yield

$$\boldsymbol{F}(f) = [h'_{B11}(f), \ldots, h'_{BM1}(f), h'_{F12}(f), \cdots h'_{F1N}(f)]^T. \tag{3.13}$$

Based on the frequency response at the receiver side, the correlation matrix can be expressed as follows:

$$\boldsymbol{R}_{FF} = \overline{\boldsymbol{F}(f)\boldsymbol{F}(f)^H} \left(f_{min} < f < f_{max} \right), \tag{3.14}$$

where f_{min} and f_{max} represent the frequency ranges that contain the influence of the vital signs, and $\{\cdot\}^H$ represents the Hermitian transposition. Subsequently, eigenvalue decomposition is applied to the correlation matrix as follows:

$$\boldsymbol{R}_{FF} = \boldsymbol{U}\boldsymbol{D}\boldsymbol{U}^H, \tag{3.15}$$

$$\boldsymbol{U} = [\boldsymbol{u}_1, \ldots, \boldsymbol{u}_L, \ldots, \boldsymbol{u}_{M+N-1}], \tag{3.16}$$

$$\boldsymbol{D} = \mathrm{diag}\left[\lambda_1, \ldots, \lambda_L, \ldots, \lambda_{M+N-1}\right], \tag{3.17}$$

where $\boldsymbol{U}$ is an eigenvector matrix, and $\boldsymbol{D}$ is a diagonal eigenvalue matrix, where $\lambda_1 \geq \ldots \lambda_L \geq \ldots \geq \lambda_{M+N-1}$. Finally, the living-body position is identified by finding the peak in the 2-dimensional MUSIC spectrum, where the computed steering vectors are defined similarly to (3.12).

Table 3.1: Simulation condition

Antenna element	Horizontal patch antenna
Number of Tx	4
Number of Rx	4
Angle of the antenna	45
Element spacing d, [m]	0.5λ
Frequency used [GHz]	2.47125
Distance between Tx and Rx [m]	8
Measurement area [m^2]	8×8
Sampling frequency [Hz]	250
Height of antenna, h [m]	1.0
Observation time [s]	30
Number of targets	1
Frequency error, $(f_1 - f_2) = \Delta f$ [Hz]	50
Number of measurement positions	64
Extracted frequency range [Hz]	$f_{min} = 0.1$ (lowest), $f_{max} = 5.0$ (highest)

(a) Without phase adjustment   (b) With phase adjustment
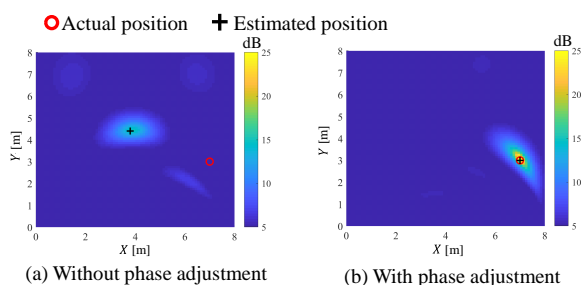
Figure 3.2: Example of the MUSIC spectrum for target localization (without and with phase correction).
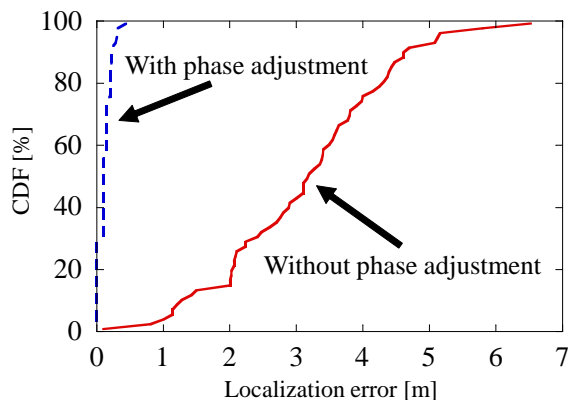

Figure 3.3: CDF of the localization error (without and with phase correction).

3.3   Simulation

3.3.1   Simulation condition

To verify the fundamental behavior of the proposed combined channel and whether it can be used for positioning similar to MIMO radars, we introduced a simple simulation where only the path by way of

the target and the direct path between the stations are considered. In contrast, realistic and complicated electromagnetic behaviors, such as path loss, radar cross section of the target, and multipath, were neglected.

Table 3.1 lists the simulation conditions used in this study. There are four transmitting and receiving antennas on both sides, that is, $N = M = 4$. The distance between the transmitter and receiver was 8 m, and the measurement area was assumed to be 8×8 m^2. The height of the antenna was set to 1.0 m, and the element spacing for both the transmitter and receiver was 0.5λ, where λ represents the wavelength. Time-variant channels were observed for over 30 seconds for each observation, and the snapshot frequency of the SIMO channels was 250 Hz. The SNR was set to 5 dB, where the noise was Gaussian white. We assumed the presence of a single living body, and the direct path channel between the transmitter and receiver was also considered; however, multipath components were not considered. The data were collected from 64 trials with random target positions. The channel with 50 Hz frequency errors was then calculated, and the spectral window to observe the vital sign ranges from 0.1 to 5 Hz.

3.3.2 Simulation results

Fig.3.2 shows an example of the MUSIC spectrum for target localization. The red circles and black crosses represent the actual and estimated positions, respectively. Fig.2 (a) shows the spectrum without phase-error correction. It failed to estimate the target because the phase error caused severe degradation in detection performance. By applying the proposed method, the peak value of the spectrum successfully appears at the target's actual location, as shown in Fig. 2 (b). Fig.3.3 shows the cumulative distribution function (CDF) of the localization error. The results showed that the 90-percentile errors with and without phase correction were 0.30 m and 4.42 m, respectively, which indicates that the proposed method can localize a single target position with significantly high accuracy.

3.4 Measurement

To further verify whether the proposed roundtrip SIMO channel could estimate the targets' position in realistic environments, an experiment was carried out in an actual multipath indoor room to verify the effect of realistic and complicated electromagnetic behaviors.

3.4.1 Measurement conditions

Fig.2.5 and Table 4.1 show the experimental condition and system overview of this work. 4×4 MIMO bidirectional channels were measured, and only $M + N - 1 = 7$ paths were retrieved from the forward

Table 3.2: Experimental condition

| Antenna element	Square microstrip antenna arrays
Polarization	Vertical
Number of Tx	4
Number of Rx	4
Distance between Tx and Rx [m]	4
Element spacing, d [mm]	56 (0.5λ)
Angle of the antennas	45
Frequency used [GHz]	2.47125
Measurement area [m^2]	4×4
Sampling frequency [Hz]	100
Antenna height, h [m]	1
Observation time [s]	60
Number of targets	$1 \sim 2$
Distance between targets [m]	1.4
Number of measurement points	16
Extracted frequency range [Hz]	$f_{min} = 0.02$ (lowest), $f_{max} = 7.0$ (highest)
Frequency error, $(f_1 - f_2) = \Delta f$ [Hz]	0, 0.3, 10
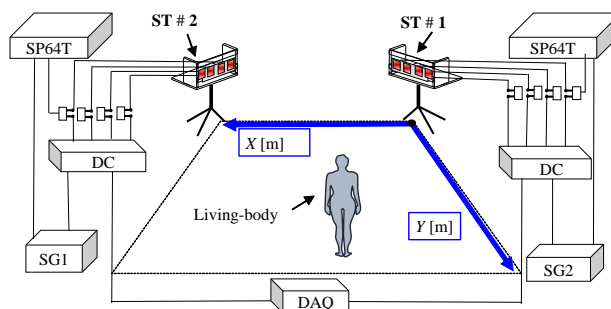
Figure 3.4: System overview.
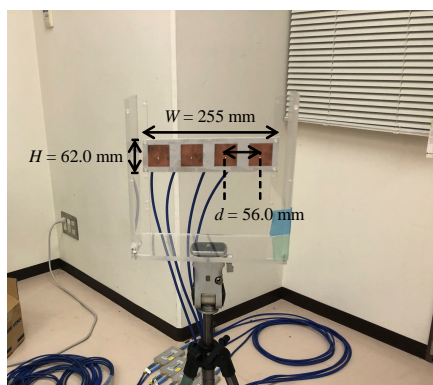
Figure 3.5: Dimensions of the used antenna array.

(from station #1 to #2) and backward (from station #2 to #1) channels to test the proposed method. The distance between stations #1 and #2 was 4 m, and the transmitter and receiver were oriented at 45 degrees to the monitoring area. The antenna height was set to 1.0 m. The time-variant channels were
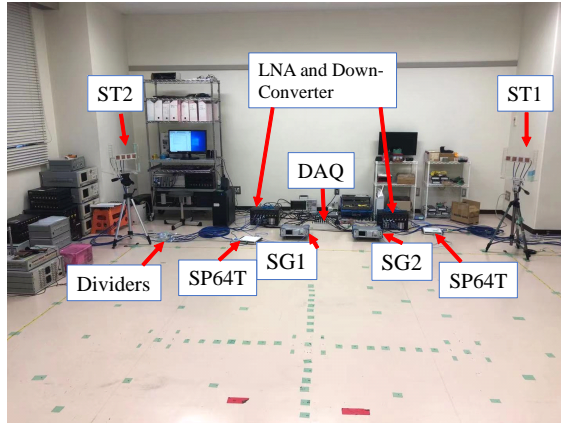
Figure 3.6: Measurement setup.
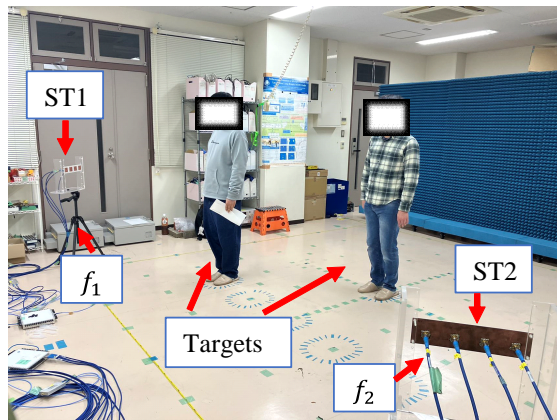
Figure 3.7: Measurement environment.

measured over 60 seconds for each observation, and the snapshot frequency of the SIMO channels was set to 100 Hz. To test various frequency differences, two signal generators (SGs) were independently used to provide CW signals to both the transmitter and receiver sides. The frequency was manually changed, and the frequency difference between the two stations in this trial was set to $f_1 - f_2 = \Delta f =$ 0, 0.3, and 10 Hz.

3.4.2 Experimental environment

Fig.3.5 shows the dimensions of the used antenna array. The dimensions of the 4-element square microstrip antenna arrays with PTFE substrate are as follows: length $H = 62.0$ mm, width $W = 255$ mm, and element spacing $d = 56.0$ mm, and the thickness of the PTFE substrate is 1.6 mm,

Fig.2.4 and 2.6 show the measurement environment. The measurements were performed in an indoor environment containing walls, desks, etc. The measurement area was 4×4 m^2, and the SGs provided

Figure 3.8: Temporal response of the SIMO channel with and without phase adjustment.
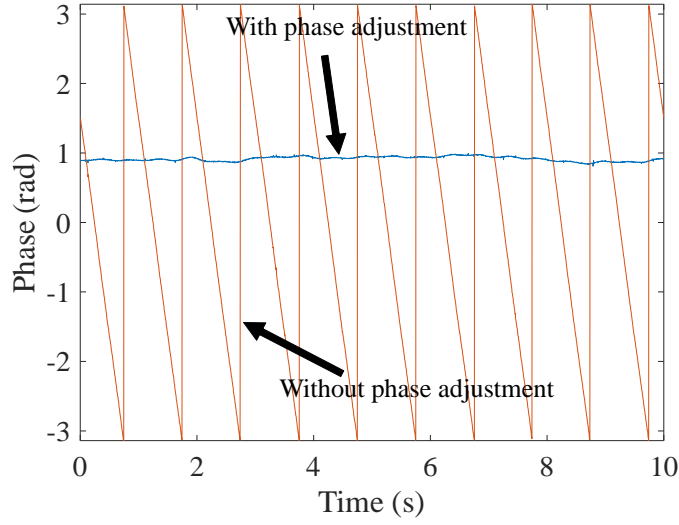
continuous CW signals near 2.47125 GHz on both the transmitter and receiver sides. The receiver requires an RF CW signal to down-convert the received signals into baseband signals. A single-pole 4-throw (SP4T) switch is connected to four two-port dividers. The received signals were input to a down-converter (DC) unit using a low-noise amplifier (LNA). The down-converter baseband signals $(I_1, Q_1, \sim I_8, Q_8)$ were then digitized and recorded by the data acquisition unit (DAQ). Multiple targets (up to two) were placed at 16 different measurement points. The distance between the two targets was set to be greater than or equal to 1.4 m because the radar could not distinguish excessively close targets. Finally, the Doppler-shifted components from 0.02 to 7.0 Hz in the baseband signals were obtained to remove the undesirable components. Therefore, only the fluctuating components produced by vital sign movements were observed. All the experimental procedures were approved by the Ethics Committee of Iwate University, Japan (admission number: #202019).

3.4.3 Experimental results

Fig.**??** shows the temporal response of h_{F11} with and without phase adjustment. When a frequency difference exists between two oscillators, the response without the phase adjustment technique incurs a rapid phase rotation. This phase rotation severely degrades the localization performance. By applying the proposed method, the phase rotation was fixed, and the fluctuation of the observed signal became relatively smooth.

Fig.3.9 shows an example of the MUSIC spectrum for both MIMO and the proposed SIMO channel
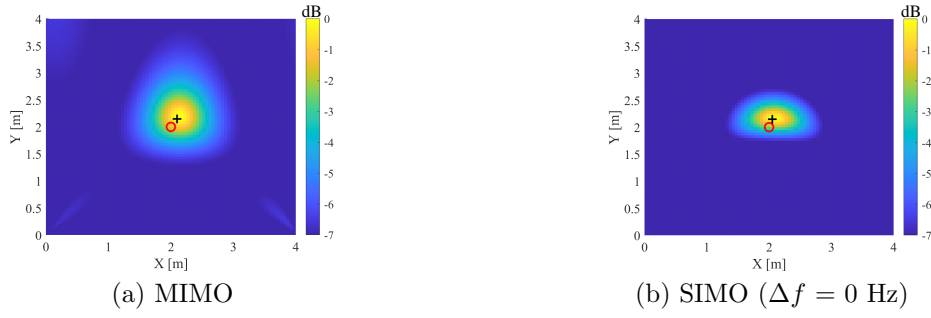
47

(a) MIMO

(b) SIMO ($\Delta f = 0$ Hz)

Figure 3.9: Example of the MUSIC spectrum for MIMO and proposed SIMO ($\Delta f = 0$ Hz) single target localization results.

(a) SIMO ($\Delta f = 0.3$ Hz)
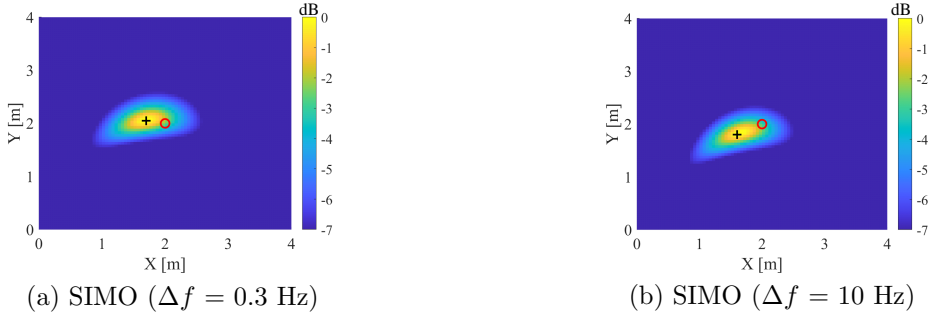

(b) SIMO ($\Delta f = 10$ Hz)

Figure 3.10: Example of MUSIC spectrum single target localization results with various frequency errors (MIMO vs. SIMO, $\Delta f = 0, 0.3, 10$ Hz).

(without phase error) target localization. As shown in Fig.3.9 (a) and (b), the target stood at position (2, 2) m; both of the peak values of the spectrum appear near the actual location of the target. This implies that the proposed merged SIMO channel ($\Delta f = 0$ Hz) and the MIMO channel can localize the target.

Fig.3.10 shows examples of MUSIC spectra by the proposed method with various frequency errors. When the frequency error Δf between two individual oscillators is small and close to the vital sign frequency, that is, $\Delta f = 0.3$ Hz, the signal processing at the receiver side may also easily eliminate the desired Doppler shift due to the targets, which degrades target localization. To test and verify this situation, when the frequency difference Δf is close to vital sign frequency, the proposed method can successfully estimate the target position by retaining the vital sign, as shown in Fig.3.10 (a). In addition, we tested and verified a situation where there is a larger frequency error($\Delta f = 10$ Hz) to consider a low-cost system with poor clock accuracy in the transmitter and receiver. As shown in Fig.3.10 (b), when larger frequency errors exist, the proposed method could still estimate the target location successfully. This result indicates that the proposed method can successfully localize the target position even when two stations have various frequency differences.
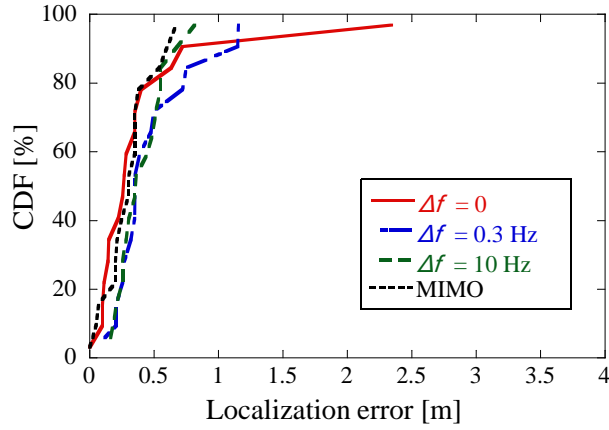
Figure 3.11: CDF of single target's localization error with various frequency differences.

(a) MIMO

(b) SIMO ($\Delta f = 0$ Hz)

(c) SIMO ($\Delta f = 0.3$ Hz)

(d) SIMO ($\Delta f = 10$ Hz)
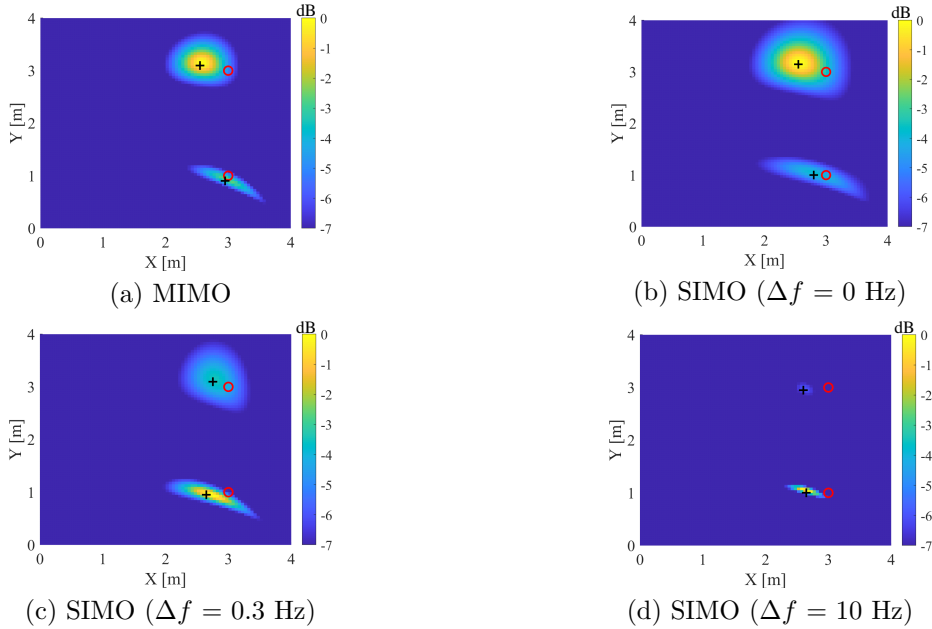
Figure 3.12: Example of MUSIC spectrum for 2-targets' localization with various frequency errors (MIMO vs. SIMO, $\Delta f = 0, 0.3, 10$ Hz.)

Fig.3.11 shows the CDF of the localization error with various frequency differences and MIMO channel estimation. As shown in the figure, when the frequency errors were $\Delta f = 0.3$ and 10 Hz, 50% of location errors were 0.35 m and 0.36 m, respectively. Moreover, when the frequency difference was $\Delta f = 0$ Hz, 50% of the location errors were 0.26 m, and the proposed method can successfully estimate target localization as well as MIMO (50% of location errors were 0.30 m). Even when various frequency errors exist, the proposed method can localize the single target position with high accuracy by adjusting the phase between forward and backward SIMO channels.

Figure 3.13: CDF of 2-targets' localization error with various frequency differences.

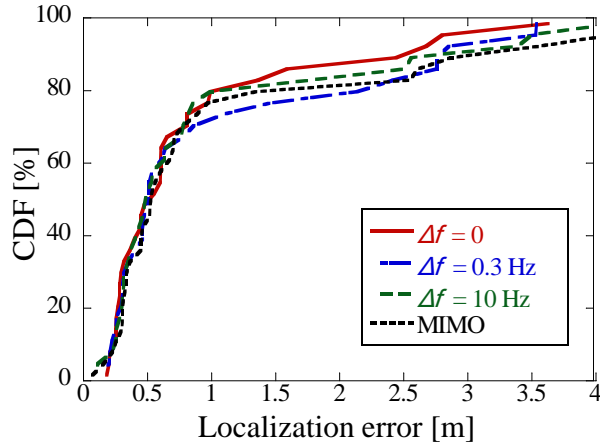The feature of the proposed method is its capability to estimate the position of both single and multiple targets because the roundtrip channel contains more information than a one-way SIMO channel. To verify this assumption, we also performed multiple target (up to two) detections in the same environment. Fig.3.12 shows an example of MUSIC spectrum for 2-targets' localization of MIMO and proposed SIMO with various frequency errors. In this example, the two targets were at positions (3,1) m and (3,3) m. As shown in Fig.3.12 (a), the MIMO channel can localize the targets' position without any issue because it has more channel information. Similarly, in the bidirectional SIMO channel shown in Fig.3.12 (b), (c), and (d), the peak values of both spectra appear near the targets' exact locations in each different scenario.

Fig.3.13 shows the CDF of the localization error with various frequency differences compared with full MIMO radar. The results of the 50% localization errors with various frequency differences for the proposed bidirectional SIMO and MIMO channel localizations were within 0.50 m. These results confirm that the proposed method can identify the locations of multiple targets (up to two) as accurately as the MIMO configuration.

3.5 Conclusion

This chapter proposed multiple human-body localization using roundtrip SIMO channels. The phase-adjustment method between the two stations has been discussed, and a target estimation method using the merged SIMO channel has been introduced. A simulation demonstrated that the proposed approach could accurately localize a single target position. An experiment with multiple indoor targets (up to two) was conducted to assess both the full-MIMO and the proposed SIMO conditions. By analyzing

the results, we found that 50% of the localization errors of both methods were all within 0.50 m. They demonstrated that even when two stations have different frequency offsets, the proposed SIMO approach can localize multiple target positions with excellent accuracy, similar to the MIMO radar, which can be easily implemented using COTS devices.

Chapter 4

ToF-based Positioning Technique and Its Evaluation Using Real Wi-Fi Stations

In this chapter, we introduce a living-body positioning technique that integrates Time-of-flight (ToF) and DoD utilizing real Wi-Fi stations. To realize a low-cost radar system that is well-suited for IoT-based applications, we assume that our Wi-Fi station has multiple transmit antennas and only a single receive antenna available. Then, the observed MISO channel is applied with a phase error correction method. Following this procedure, we discuss the position estimation method, which combines ToF and DoD. An experiment using real Wi-Fi stations is carried out, and finally, we analyze the measurement results of the localization.

4.1   Theoretical model of localization using ToF and DoD

4.1.1   phase correction method for bistatic MISO channel

As discussed in Chapter One, leveraging COTS devices can help reduce expenses in radar systems. To achieve a low-cost system suitable for IoT-based radar, Chapter 3 assumed the presence of two stations (transmitter and receiver stations), each equipped with multiple antennas. However, only a single antenna could transmit and receive, while the other antennas could only receive.

In this chapter, we continue to utilize two widely separated stations (transceivers). However, we assume that our station has multiple transmit antennas and only a single receive antenna available, resulting in the utilization of a Multiple Input Single Output (MISO) channel for localization. However, because the transceivers are widely separated and are COTS devices, inaccuracies in the local oscillator can cause frequency errors in both the transmitter and receiver, thereby affecting the radar's localization

capabilities. Hence, we apply a phase elimination technique suitable for the MISO channel as described below.

The observed MISO channel with the time-varying phase rotation Δf is defined as

$$\boldsymbol{h}(t) = [h_1(t), \cdots, h_{M_T}(t)] \exp(j\Delta f(t)). \tag{4.1}$$

where $\{\cdot\}^T$ represents the transposition, M_T is the number of the transmitter, and t represents the time of the channel observation. This also can be rewritten as

$$\boldsymbol{h}_(t) = (h_{\text{fix}} + h_{\text{vital}}(t)) \exp(j\Delta f(t)) + h_{\text{noise}}(t)$$
$$= h_{\text{fix}} \exp(j\Delta f(t)) + h_{\text{vital}}(t) \exp(j\Delta f(t)) + h_{\text{noise}}(t). \tag{4.2}$$

Here, $\boldsymbol{h}_{\text{fix}}$ and $\boldsymbol{h}_{\text{vital}}$ represent fixed channel and reflected micro-Doppler channel due to the human body's displacement, respectively. $\boldsymbol{h}_{\text{noise}}$ is the noise component due to the thermal noise. Note that $\boldsymbol{h}_{\text{fix}}$ mainly consists of the direct path because we assume that the transmitter and the receiver are in a line-of-sight (LOS).

Next, the observed MISO channel with the phase error is applied to the phase error elimination method as

$$\boldsymbol{h}_{\text{cal}}(t) = \boldsymbol{h}(t) \otimes \exp^{j\angle(h_{\text{fix}} \oslash h(t))} \tag{4.3}$$

where $\otimes$ represents the Hadamard product, and $\oslash$ represents the Hadamard division. By using this method, a new MISO channel without the phase error $\boldsymbol{h}_{\text{cal}}(t)$ is calculated.

However, due to the limitations of the antenna, this MISO channel can only observe the direction of departure; therefore, it is not suitable for estimating the position of the human body.

4.1.2 Position estimation method of combing ToF and DoD

As we discussed above, only the DoD information is not enough to estimate the target's position, therefore, we apply the localization method by combining DoD and ToF. In this study, we utilize Orthogonal Frequency Division Multiplexing (OFDM) signals, a widely employed modulation technique in modern communication systems, particularly in wireless communication standards such as Wi-Fi. Additionally, we can acquire propagation path information for each frequency subcarrier. As shown in Fig.4.1, incoming waves reach the array antenna with propagation path length S_{ToF} and departure angle θ_{DoD}. Consequently, we can estimate distance information based on ToF from the propagation path data in the frequency domain, enabling localization by combining it with DoD information. The mathematical expression for this method is discussed below.
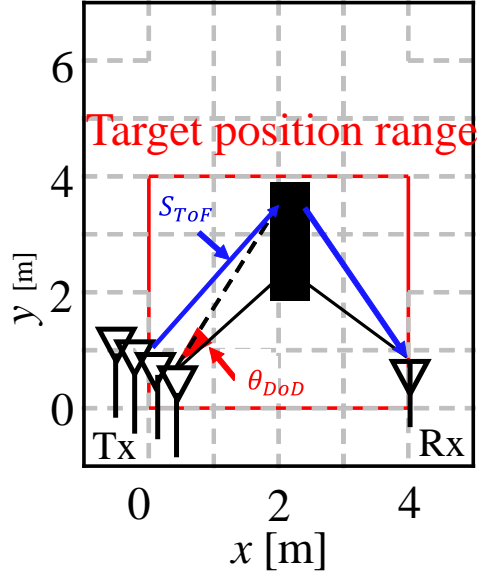
Figure 4.1: Concept of the MISO channel localization.

$$\boldsymbol{H}(t) = \begin{pmatrix} h_{11}(t) & \cdots & h_{1M_{(T)}}(t) \\ \vdots & \vdots & \ddots & \vdots \\ h_{K1}(t) & \cdots & h_{KM_T}(t) \end{pmatrix} \tag{4.4}$$

here, K represents the total number of frequency subcarriers, while M_T denotes the number of transmitting antenna elements. This channel matrix represents propagation path information in the spatial $\times$ frequency domain. Note that each column of this channel matrix is subjected to the phase error elimination technique discussed above.

Next, this channel matrix is vectorized, and in order to exclude unwanted paths such as the direct path, and extract only the vital signs, it is Fourier transformed as

$$\boldsymbol{h}_{\mathrm{f}}(f) = \mathrm{vec}(\mathcal{F}[\boldsymbol{H}(t)]) \tag{4.5}$$

Then the correlation matrix is calculated as

$$\boldsymbol{R}_{\mathrm{f}} = E[\boldsymbol{h}_{\mathrm{f}}(f)^{\mathrm{H}} \boldsymbol{h}_{\mathrm{f}}(f)] \tag{4.6}$$

Finally, we use the Capacitive and Advanced Processing of Neurons (CAPON) method to search the peak value of the spectrum. Since the observed channel consists of propagation distance S_{ToF} and departure angle θ_{DoD}, it is necessary to calculate a mode vector orthogonal with Capon. Here, the
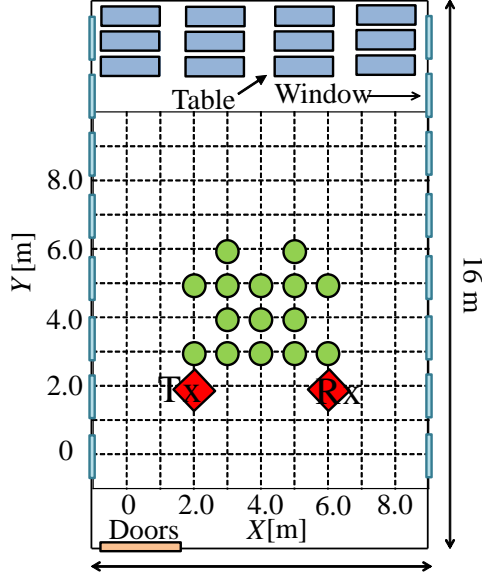
54

Figure 4.2: System overview

mode vector $\boldsymbol{A}(\boldsymbol{S}, \boldsymbol{\theta})$ define as

$$\boldsymbol{a}(S, \theta) = \begin{pmatrix} a_{11}(S, \theta) & \cdots & a_{1M(T)}(S, \theta) \\ \vdots & \vdots & \ddots & \vdots \\ a_{K1}(S, \theta) & \cdots & a_{KM_T}(S, \theta) \end{pmatrix} \tag{4.7}$$

Then, the Capon spectrum is calculated as

$$P_{\text{Capon}} = \frac{1}{\boldsymbol{a}^H \boldsymbol{R}_{\text{f}}^{-1} \boldsymbol{a}}. \tag{4.8}$$

By identifying peaks present in this spectrum, we estimate the departure angle θ_{DoD} and the propagation distances S_{ToF} of the signals passing through the target. Finally, assuming that the positions of the transmitting and receiving antennas are known, we can geometrically determine the position of the target based on the departure angle and propagation distance information.

4.2   measurement evaluation

In this chapter, we discuss the experiment condition and analyze the measurement results by using real Wi-Fi-based radar.

4.2.1   Measurement conditions and environment

Table 4.1 and Fig.4.2 illustrate the system overview and measurement conditions, while Fig.4.3 depict the measurement environment. For this experiment, two Wi-Fi Access Points (APs) compatible with IEEE 802.11 ax served as the transmitter and receiver. The transmitter side employed 4 antenna

Figure 4.3: Measurement environment

Table 4.1: Experimental condition

Number of Tx	4
Number of Rx	1
Distance between Tx and Rx [m]	4
Angle of the antennas	45
Frequency used [GHz]	2.412
Measurement area [m^2]	4×4
Sampling frequency [Hz]	10
Antenna height, h [m]	1
Observation time [s]	25.6
Number of targets	1
Number of subcarrier	53
Number of measurement points	15×4
Extracted frequency range [Hz]	$f_{min} = 0.1$ (lowest), $f_{max} = 4.0$ (highest)

elements, whereas only 1 antenna element was used on the receiver side. The distance between the transmitter (Tx) and receiver (Rx) was 4 meters, with both oriented at 45 degrees to the monitoring area, and the antenna height was set to 1.0 meter. Time-variant channels were measured over 25.6 seconds for each observation, with a snapshot frequency of 10 Hz for the Multiple Input Single Output (MISO) channels. The frequency band used was 20 MHz, with a total of 53 subcarriers, and the Wi-Fi signals near 2.412 GHz were utilized. Measurements were conducted indoors, encompassing walls, desks, etc., within a 4×4 square meter area. There were 15 measurement locations, and 4 participants were involved. Only one participant entered the environment, and measurements were repeated 60 times in total. To extract Doppler shifts resulting from human body surface displacement, the participant performed stand-stepping. The extracted frequency was 0.1 Hz for the lowest and 4 Hz for the highest.
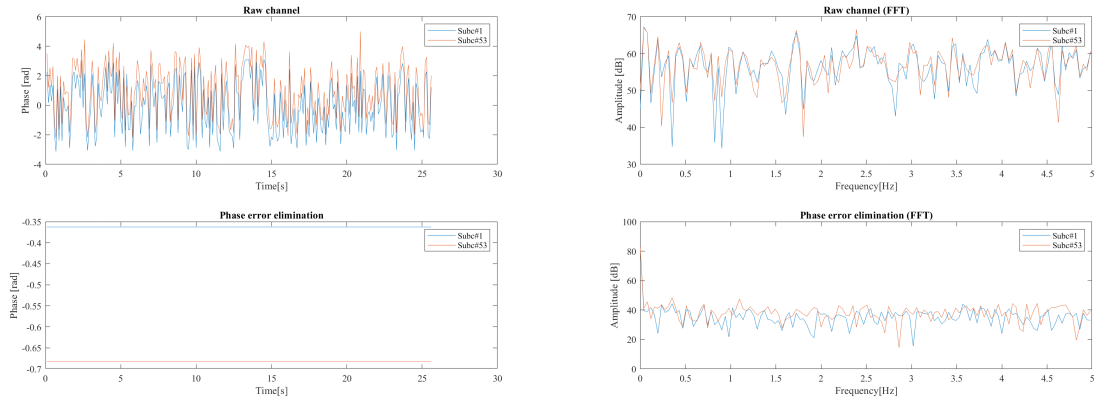
Figure 4.4: Temporal response of the MISO raw channel VS phase error elimination method channel (target position(2,3))

Figure 4.5: An example of Capon spectrum of the ToF estimation (target position(2,3))

Figure 4.6: ToF estimation for all targets.
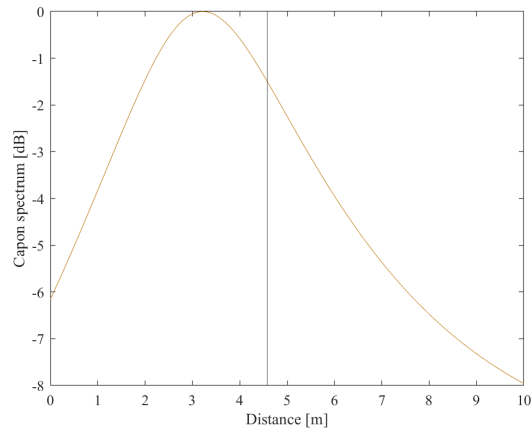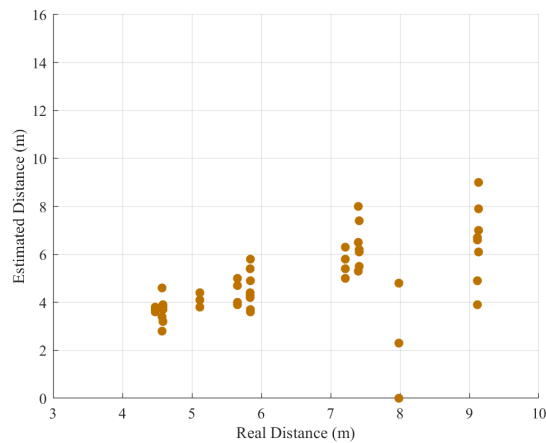
4.2.2 Measurement results

Figure 4.4 depicts the temporal response of the MISO raw channel compared to the phase error elimination method channel (target position(2,3)). As shown in this figure, in the first row, the measured
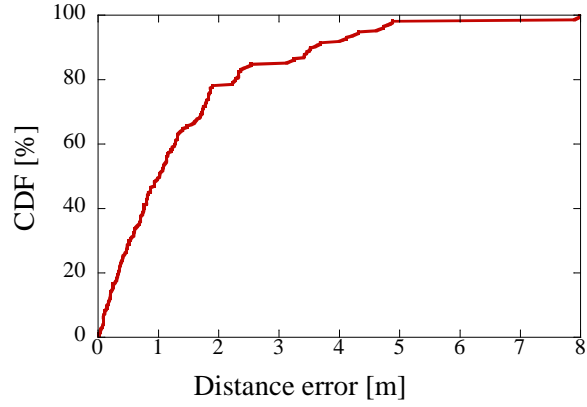
Figure 4.7: CDF of the ToF estimation.

(a) DoD and ToF estimation
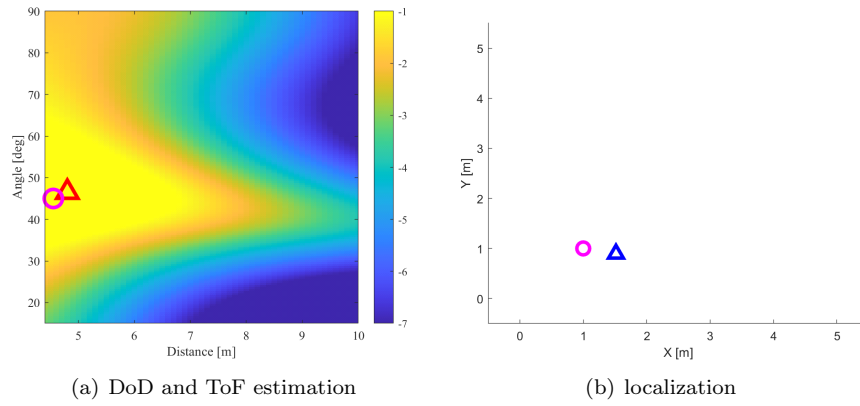
(b) localization

Figure 4.8: Example of DoD and ToF estimation and localization.

raw channel's phase information changes rapidly and is very noisy. Despite applying the FFT to extract vital signs, observing the Doppler component from this channel is extremely difficult. However, after applying the phase error elimination technique, in the second row, the phase rotation becomes very smooth, and following the FFT, the vital signs can be successfully observed.

Figure 4.5 displays the Capon spectrum of the ToF estimation results (target position(2,3)). As shown in this figure, the actual distance for ToF is 7.14 meters, while the peak value of the estimated distance for ToF appears at 6.48 meters. This indicates that the ToF is accurately estimated in this result.

Figure 4.6 illustrates the results of the ToF estimation for all targets. As depicted in this figure, the estimated distances mostly align closely with the real distances, indicating the success of the ToF estimation.

Figure 4.7 shows the Cumulative Distribution Function (CDF) of the ToF estimation. By looking

(a) DoD and ToF estimation   (b) Localization
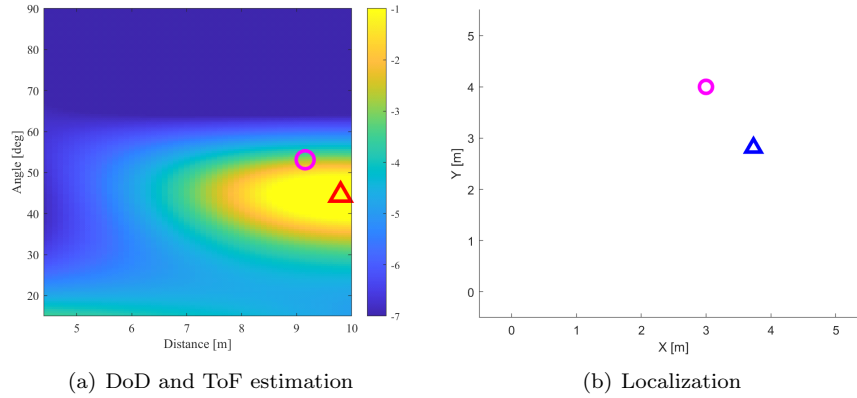
Figure 4.9: Example of DoD and ToF estimation and localization.
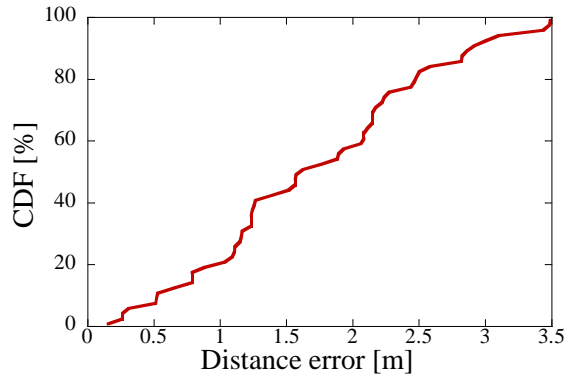
Figure 4.10: CDF of the localization error.

at the 50% of the distance error, the distance error is 1.02 m.

Figure 4.8(a) displays the Capon spectrum for both DoD and ToF estimation, while 4.8(b) showcases the localization result. The target position is (1,1). The pink circle represents the actual position, and the red rectangle represents the estimated position. As shown in this figure, the actual DoD is 42.5 degrees, and the actual ToF is 4.55 meters. The estimated DoD is 46.5 degrees, and the estimated ToF is 4.80 meters. The estimated location for the target is (1.4, 0.9) meters.

Figure 4.9(a) demonstrates another example of the Capon spectrum for both DoD and ToF estimation, while Figure 4.9(b) presents the localization result. The target position is (3,4). As depicted in this figure, the actual DoD is 52.4 degrees, and the actual ToF is 9.1 meters. The estimated DoD is 44.5 degrees, and the estimated ToF is 9.80 meters. The estimated location for the target is (3.8, 2.9) meters.

Figure 4.10 illustrates the CDF of the localization error results. As depicted in this figure, the 50% of the distance error is 1.57 meters. This outcome suggests that the combination of DoD and ToF positioning methods is effective, and Wi-Fi-based radar can successfully estimate the target's location with reasonable accuracy.

4.3 Conclusion

In this chapter,we investigates a living-body positioning technique that integrates ToF and DoD utilizing real Wi-Fi stations.To realize a low-cost radar system that is well-suited for IoT-based applications, we assume that our Wi-Fi station has multiple transmit antennas and only a single receive antenna available. In this experiment, Wi-Fi signals are used,and ranging is performed by calculating ToF from the frequency characteristics of the Channel State Information (CSI) retrieved from the subcarrier channels.Then, the direction of departure information is calculated. Next, the MISO channel phase error due to the clock difference between the transmitter and receiver is removed using the frequency calibration technique. Finally, the channel is Fourier-transformed, and the locations of living bodies are estimated. The experimental results confirm that our Wi-Fi-based radar could successfully localize the target's position.

Chapter 5

Summary

Recently, the COVID-19 pandemic has had a widespread impact, highlighting the issue of staying indoors demand. Furthermore, with the increasing number of elderly individuals living alone, there has been a corresponding rise in the incidence of accidental falls in elderly households, and the concerning problem of isolated deaths among the need for direct contact with the human body handicaps the latter global scale. As a result, there is a growing need for systems that can efficiently monitor the safety of the elderly. In addressing this demand, the use of wireless biomedical sensors such as bistatic MIMO and SIMO radar for safety monitoring has garnered significant attention. Unlike traditional safety monitoring systems such as video cameras and wearable devices, this approach does not violate privacy, and body contact is unnecessary. Furthermore, it can localize the human body's position. To reduce the cost of the radar system and suit the bistatic bio-radar, it is desirable to use commercially available imperfect RF devices. However, in such a COTS-based bistatic system, the transmitter and receiver are physically separated when utilizing two stations as transceivers because of the limitations of clock accuracy in their individual oscillators, where the frequencies of each station are inherently different. The phase error between the two stations strongly affects the localization accuracy. Therefore, research on the localization of the human bodies using array-based bio-radar with imperfect RF devices is needed.

In chapter one, the technical background of modern detection systems is introduced, and the existing problems with these systems are discussed. Then the effectiveness of the bistatic MIMO radar in safety confirmation applications is mentioned. Also, the realization of localization using bistatic SIMO radar is discussed. To reduce the cost problems, the problems in bistatic MIMO and SIMO radar using imperfect RF devices for localization are listed. Among the raised problems, the target of this study was frequency offset elimination between the transmitter and receiver and multitarget detection concerning the importance of realizing this system.

In chapter two, we present and experimentally evaluate a frequency error elimination technique suitable for unsynchronized bistatic MIMO radar for human-body detection. First, a mathematical expression of human body localization using bistatic MIMO radar is presented. Then the direct path is used to eliminate the phase error created by the frequency difference between the transmitter and receiver. A new Doppler-shifted component of the MIMO channel without phase error is derived, and the locations of the multiple targets are calculated by the 2-dimensional MUSIC method. Next, the results of simulations that examine frequency error versus power ratios are discussed to illustrate the effectiveness of the proposed method. An experiment is carried out in an indoor multipath-rich environment. To emulate the unsynchronized condition, the transmitter and receiver use independent SGs. One to six targets are tested. The experiments demonstrate that our unsynchronized radar system can identify the locations of multiple targets with high accuracy.

In chapter three, we introduce an accurate human-body localization using a roundtrip SIMO channel for biomedical health monitoring applications. Two commercial off-the-shelf stations are assumed to be used to realize a low-cost radar system, where each station has only a single transmitting RF-frontend among the multiple antennas. The proposed technique consists of two important ideas. First, roundtrip channels between two stations are merged to perform a simultaneous positioning of the multiple targets, where multiple DoA information at both stations are jointly used. Second, a frequency error elimination technique for the roundtrip channel between two stations is proposed. The performance of the proposed SIMO radar system for human-body localization is thoroughly evaluated through both numerical simulations and experimental analysis. The simulation results confirmed that the single target's localization error for the proposed method was 0.30 m. In the experiment, two targets were simultaneously localized in an indoor multipath-rich environment with various frequency errors. The localization results verified that our proposed method could localize the targets' position within 0.50 m error, even when two stations have various frequency errors. In chapter four, we experimentally evaluate the human-body positioning through the MISO channel, utilizing real Wi-Fi devices. Localization is achieved by combining ToF and DoA.

Reference

[1] H. Sugano, T. Tsujioka, T. Inoue, S. Nakajima, S. Hara, H. Nakamura, K. Takeuchi "Clinical tests and evaluations of a wireless ECG sensor for realization of ubiquitous health care systems," Engineering in Mdicine and Biology Society(EMBC), 2010 Annual International Conference of the IEEE, pp. 2030-2033, Aug. 2010.

[2] K. Watanabe, T. Watanabe, H. Watanabe, H. Ando, T. Ishikawa, K. Kobayashi, "Noninvasive measurement of heartbeat, respiration, snoring and body movements of a subject in bed via a pneumatic method," IEEE Transactions on Biomedical engineering, vol.52, No.12, Dec. 2005.

[3] Y. Imai, K. Otsuka, Y. Kawano, K. Shimada, H. Hayashi, O. Tochikubo, M. Miyakawa, K. Fukiyama, "Japanese society of hypertension (JSH) guidelines for self-monitoring of blood pressure at home," Hypertension Research Vol. 26, No. 10, pp. 771-782, 2003.

[4] D. Rodriguez-Martin, A. Sama, C. Perez-Lopez, A. Catala, J. Cabestany, and A. Rodriguez-Molinero, "SVM-based posture identification with a single waist-located triaxial accelerometer," Expert Systems with Applications, Vol. 40, No. 18, pp. 7203-7211, Dec. 2013.

[5] J. Krumm, S. Harris, B. Meyers, B. Brumitt, M. Hale, and S. Shafer, "Multi-camera multi-person tracking for easyliving," In Proceedings Third IEEE International Workshop on Visual Surveillance, pp. 3-10, Jul. 2000.

[6] V. Ganapathi, C. Plagemann, D. Koller, and S. Thrun, "Real time motion capture using a single time-of-flight camera," In Computer Vision and Pattern Recognition (CVPR), pp. 755-762, Jun. 2010.

[7] Z. Zhang, "Microsoft Kinect sensor and its effect," IEEE Multimedia Mag., Vol. 19, No. 2, pp. 4-10, Feb. 2012.

[8] M. Nango, N. Honma, K. Nishimori, and H. Sato, "Biological activity detection method using MIMO system," *IEICE Communication Express 2(2)*, pp. 36-41, 2013.

[9] R. O. Schmidt, "Multiple emitter location and signal parameter estimation," *IEEE Transaction Antenna Propagation*. Vol. AP-34, pp. 276-280, Mar. 1986.

[10] J. Li, P. Stoica, "MIMO radar signal processing," Hoboken, NJ: wiley, 2009.

[11] F. Adib, Z. Kabelac, and D. Katabi, "Multi-person motion tracking via RF body reflections," *Computer Science and Artificial Intelligence Laboratory Technical Report*, MIT-CSAIL-TR-2014-008, Apr 26, 2014.

[12] K. Konno, N. Honma, D. Sasakawa, K. Nishimori, N. Takemura, and T, Mitsui, "Esatimating living body location using bistatic MIMO radar in multipath environment," *IEICE Trans.* Commun. Vol.J98-B, no. 11, (in press), Nov. 2015.

[13] T. Miwa, S. Ogiwara, Y. Yamakoshi, "Localization of living-bodies using single-frequency multistatic Doppler radar system," *IEICE Trans.* Commun. 2009, 9, 2468?2476.

[14] H. Yan, J. Li, and G. Liao, "Multitarget identification and localization using bistatic MIMO radar systems," *EURASIP J. Adv. in Signal Process*, vol. 2008, no. ID 283483, 2008.

[15] P. Chen, Z. Cao, Z. Chen, and C. Yu, "Sparse DOD/DOA estimation in a bistatic MIMO radar with mutual coupling effect," *Electronics*, vol. 7, no. 11, p. 341, Nov. 2018.

[16] F. Wen, Z. Zhang, and G. Zhang, "Joint DOD and DOA estimation for bistatic MIMO radar: A covariance trilinear decomposition perspective," *IEEE Access*, vol. 7, pp. 53273?53283, 2019.

[17] W. Tang, H. Jiang, and S. Pang, "Grid-free DOD and DOA estimation for mimo radar via duality-based 2d atomic norm minimization," *IEEE Access*, vol. 7, pp.827?836, 2019.

[18] S. Gong, H. Xiong, M. Peng, X. Ding, and H. Tang, "Joint DOD and DOA estimation for bistatic multiple-input multiple-output radar target discrimination based on improved unitary ESPRIT method," *IET Commun*, vol. 12, no. 12, pp. 1397?1405, Jul. 2018.

[19] A.Abudusaimi, N. Shiraki, N. Honma, T. Nakayama, S. Iizuka, "Performance evaluation of multiple human-Body localization using bistatic MIMO radar," *2019 APMC Conference*, IF-44, Sep. 2019.

[20] E. Cardillo and A. Caddemi, "A review on biomedical MIMO radars for vital sign detection and human localization," *Electronics*, vol. 9, no. 9, p. 1497, Sep. 2020.

[21] D. Sasakawa, N. Honma, T. Nakayama, and S. Iizuka, "Fast living-body localization algorithm for MIMO radar in multipath environment," *IEEE Transactions on Antennas and Propagation*, vol. 66, no. 12, pp. 7273-7281, Dec. 2018.

[22] D. Sasakawa, K. Konno, N. Honma, K. Nishimori, N. Takemura, and T. Mtsui, "Antenna array calibration for living-body radar," *IEEE Antennas Wireless Propag. Lett.*, vol. 15, pp. 246-249, 2016.

[23] M. Eineder, "Oscillator clock drift compensation in bistatic interferometric SAR," *Proc. IGARSS*, Toulouse, France, 2003, pp. 1449?1451.

[24] M. Younis, R. Metzig, and G. Krieger, "Performance prediction of a phase synchronisation link for bistatic SAR," *IEEE Geosci. Remote Sens. Lett*, vol. 3, no. 3, Jul. 2006.

[25] M. Gottinger, F. Kirsch, P. Gulden, and M. Vossiek, "Coherent full-duplex double-sided two-way ranging and velocity measurement between separate incoherent radio units," *IEEE Trans. Microw. Theory Techn*, vol. 67, no. 5, pp. 2045?2061, May 2019.

[26] D. Liang, K. Liu, H. Zhang, Y. Deng, D. Liu, Y. Chen, C. Li, H. Yue, R. Wang, "A high-accuracy synchronization phase compensation method based on Kalman filter for bistatic synthetic aperture radar". *IEEE Geosci. Remote Sens. Lett*, 2020, 17, 1722?1726.

[27] D. Liang, K. Liu, H. Yue, Y. Chen, Y. Deng, H. Zhang, G. J. C. Li, R. Wang, "An advanced non-interrupted synchronization scheme for bistatic synthetic aperture Radar," *in Proc. IEEE Int. Geosci. Remote Sens. Symp*, Jul. 2019, pp. 1116?1119.

[28] L. Yulin, Y. Jianyu, and X. Jintao, "Synchronization technology of bistatic radar system," In *Proc. Int. Conf. Commun. Circuits Syst*, pp. 2219-2221, Sep. 2006.

[29] R.Saini, R.Zuo and M.Cherniakov, "Problem of signal synchronization in space-surface bistatic synthetic aperture radar based on global navigation satellite emissions experimental results," *IEEE Radar Sonar Navig.*, vol. 4, no. 1, pp. 110-125, Feb. 2010.

[30] P. Marques, A. Ferreira, F. Fortes, P. Sampaio, H. Rebelo, and L. Reis, "Bistatic passive radar demonstrator using COTS",*NATO RTO SET-187 Specialists Meeting on Passive Radar challenges concerning theory and practice in militar applications*, Szczecin, Poland, May. 2013.

[31] R. Schmidt, "Multiple emitter location and signal parameter estimation," *IEEE Transactions on Antennas and Propagation*, Vol. 34, no. 3, pp. 276-280, Mar. 1986.

[32] H. Seki and Y. Hori, "Detection of abnormal action using image sequence for monitoring system of aged people," *The transactions of IEEJ. D, A publication of Industry Applications Society 122(2)*, pp. 182-188, Feb. 2002.

[33] H. Schneiderman and T. kanade, "A statistical method for 3D object detection applied to face and cars," *IEEE Conference on Computer Vision and Pattern Recognition*, pp. 746-751, Jun. 2000.

[34] S. Li, L. Zhu, Z. Zhang, A. Blake, H. Zhang, and H. Shum, "Statistical learning of multi-view face detection," *In European Conference on Computer Vision*, pp. 67-81, May. 2002.

[35] J. Lin and J. Salinger, "Microwave measurement of respiration," *1975 EEE-MTT-S International Microwave Symposium (MTT-S)*, pp. 285-287, May. 1975.

[36] A. Droitcour, V. Lubecke, L. Jenshan, and O. Boric- Lubecke, "A microwave radio for Doppler radar sensing of vital signs," *2001 IEEE International Microwave Symposium (MTT-S)*, pp. 175-178, May. 2001.

[37] H. Avagyan, A. Hakhoumian, H. Hayrapetyan, N. Pogosyan and T. Zakaryan, "Portable non-contact microwave Doppler radar for respiration and heartbeat sensing," *Armenian Journal of Physics*, Vol. 5, no.1, pp. 8-14, 2012.

[38] D. Naga and A. Mase, "Measurement of heat rate variability and stress evaluation by using microwave reflectometry vital signal sensing," *Review of scientific Instruments*, 81(2010) 094301.

[39] A. Mase, N. Ito, Y. Komada, A. Kobayashi, T. Shimazu, E. Sakata, and F. Sakai, " Microwave reflectometric measurement of heart-rate variability and stress evaluation," *Asia-Pacific Microwave Conference, Kaohsiung*, pp. 625-627, Dec. 2012.

[40] Y. D. Zhang, M. G. Amin, and B. Himed, "Joint DOD/DOA estimation in MIMO radar exploiting time-frequency signal representations," *EURASIP Journal on Advances in Signal Processing*, vol. 2012, no. 1, Jul, 2012.

[41] M. L. Bencheikh and Y. Wang, "Joint DOD-DOA estimation using combined ESPRIT-MUSIC approach in MIMO radar," *Electronics Letters*, vol. 46, no. 15, pp. 1081?1083, 2010.

[42] N.Shiraki, N.Honma, K.Murata, T.Nakayama, and S.Iizuki, "Estimation method of the number of targets using cooperative multi-static MIMO radar," *IEICE Trans. Commun*, vol.E104-B, no.12, Dec. 2021.

[43] A. Caddemi and E. Cardillo, "Optical control of gain amplifiers at microwave frequencies," *Computing and Electromagnetics International Workshop (CEM)*, Barcelona, Spain, pp. 51-52, Jun. 2017.

[44] A. Visweswaran et al., "A 145GHz FMCW-radar transceiver in 28nm CMOS," *IEEE Int. Solid-State Circuits Conf. (ISSCC)* Dig. Tech. Papers, San Francisco, CA, USA, pp. 168-169, Feb. 2019.

[45] M. Muragaki, S. Okumura, K. Maehara, T. Sakamoto, M. Yoshioka, K. Inoue, T. Fukuda, H. Sakai, and T. Sato, "Noncontact respiration monitoring of multiple closely positioned patients using ultra-wideband array radar with adaptive beamforming technique," *in Proc. IEEE Int. Conf. Acoust., Speech Signal Process. (ICASSP)*, New Orleans, LA, USA, pp. 1118?1122, Mar. 2017.

[46] S. M. M. Islam, O. Boric-Lubecke, and V. M. Lubekce, "Concurrent respiration monitoring of multiple subjects by phase-comparison monopulse radar using independent component analysis (ICA) with JADE algorithm and direction of arrival (DOA)," *IEEE Access*, vol. 8, pp. 73558?73569, Apr. 2020.

[47] Y. Wang, Q. Liu, and A. E. Fathy, "Simultaneous localization and respiration detection of multiple people using low cost UWB biometric pulse Doppler radar sensor," *in IEEE MTT-S Int. Microw. Symp. Dig.*, Montreal, QC, Canada, pp. 1?3, Jun. 2012.

[48] C. Chen et al., "TR-BREATH: Time-reversal breathing rate estimation and detection," *IEEE Trans. Biomed. Eng.*, vol. 65, no. 3, pp. 489?501, Mar. 2018.

[49] D. Zhang, Y. Hu, Y. Chen, and B. Zeng, "BreathTrack: Tracking indoor human breath status via commodity WiFi," *IEEE Internet Things J.*, vol. 6, no. 2, pp. 3899?3911, Apr. 2019.

[50] H. Shen et al., "Respiration and heartbeat rates measurement based on autocorrelation using IR-UWB radar," *IEEE Trans. Circuits Syst. II, Exp. Briefs.*, vol. 65, no. 10, pp. 1470?1474, Oct. 2018.

[51] P. Cao, W. Xia, M. Ye, J. Zhang, and J. Zhou, "Radar-ID: Human identification based on radar micro-Doppler signatures using deep convolutional neural networks," *IET Radar, Sonar Navigat.*, vol. 12, no. 7, pp. 729?734, Jul. 2018.

[52] Y. Kim and H. Ling, "Human activity classification based on microDoppler signatures using a support vector machine," *IEEE Trans. Geosci. Remote Sens.*, vol. 47, no. 5, pp. 1328?1337, May 2009.

[53] C. Karabacak, S. Z. Gurbuz, A. C. Gurbuz, M. B. Guldogan, G. Hendeby, and F. Gustafsson, "Knowledge exploitation for human micro-Doppler classification," *IEEE Geosci. Remote Sens. Lett.*, vol. 12, no. 10, pp. 2125?2129, Oct. 2015.

[54] B. Tekeli, S. Z. Gurbuz, and M. Yuksel, "Information-theoretic feature selection for human micro-Doppler signature classification," *IEEE Trans. Geosci. Remote Sens.*, vol. 54, no. 5, pp. 2749?2762, May 2016.

[55] Y. Kim and T. Moon, "Human detection and activity classification based on micro-Doppler signatures using deep convolutional neural networks," *IEEE Geosci. Remote Sens. Lett.*, vol. 13, no. 1, pp. 8?12, Jan. 2016.

[56] D. Sasakawa, N. Honma, T. Nakayama, and S. Iizuka, "Fast living-body localization algorithm for MIMO radar in multipath environment," *IEEE Trans. Antennas Propag.*, vol. 66, no. 12, pp. 7273?7281, Dec. 2018.

[57] S. Hasebe, D. Sasakawa, K. Kishimoto, and N. Honma, "Simultaneous detection of multiple targets' vital signs using MIMO radar," *in Proc. Int. Symp. Antennas Propag. (ISAP).*, pp. 1?2, Oct. 2018.

[58] M. Nosrati, S. Shahsavari, S. Lee, H. Wang, and N. Tavassolian, "A concurrent dual-beam phased-array doppler radar using MIMO beamforming techniques for short-range vital-signs monitoring," *IEEE Trans. Antennas Propag.*, vol. 67, no. 4, pp. 2390?2404, Apr. 2019.

[59] X. Shang, J. Liu, and J. Li, "Multiple object localization and vital sign monitoring using IR-UWB MIMO radar," *IEEE Trans. Aerosp. Electron. Syst.*, vol. 56, no. 6, pp. 4437?4450, Dec. 2020.

[60] S. Wang et al., "A novel ultra-wideband 80 GHz FMCW radar system for contactless monitoring of vital signs," *in Proc. 37th Annu. Int. Conf. IEEE Eng. Med. Biol. Soc. (EMBC).*, pp. 4978?4981. Aug. 2015.

[61] R. Feger, C. Wagner, S. Schuster, S. Scheiblhofer, H. Jager, and A. Stelzer, "A 77-GHz FMCW MIMO radar based on an SiGe singlechip transceiver," *IEEE Trans. Microw. Theory Techn.*, vol. 57, no. 5, pp. 10020?10350, May 2009.

[62] L. Wan, X. Kong, and F. Xia, "Joint range-doppler-angle estimation for intelligent tracking of moving aerial targets," *IEEE Internet Things J.*, vol. 5, no. 3, pp. 1625?1636, Jun. 2018.

[63] T. Miwa, S. Ogiwara, Y. Yamakoshi, "Localization of living-bodies using single-frequency multi-static Doppler radar system," *IEICE Trans.* Commun. 2009, 9, 2468?2476.

[64] H. Yan, J. Li, and G. Liao, "Multitarget identification and localization using bistatic MIMO radar systems," *EURASIP J. Adv. in Signal Process*, vol. 2008, no. ID 283483, 2008.

[65] P. Chen, Z. Cao, Z. Chen, and C. Yu, "Sparse DOD/DOA estimation in a bistatic MIMO radar with mutual coupling effect," *Electronics*, vol. 7, no. 11, p. 341, Nov. 2018.

[66] F. Wen, Z. Zhang, and G. Zhang, "Joint DOD and DOA estimation for bistatic MIMO radar: A covariance trilinear decomposition perspective," *IEEE Access*, vol. 7, pp. 53273?53283, 2019.

[67] W. Tang, H. Jiang, and S. Pang, "Grid-free DOD and DOA estimation for MIMO radar via duality-based 2d atomic norm minimization," *IEEE Access*, vol. 7, pp.827?836, 2019.

[68] A. Abuduaini, N. Shiraki, N. Honma, T. Nakayama and S. Iizuka, "Frequency Error Compensation of Unsynchronized Bistatic CW- MIMO Radar for Multiple Human-Body Localization," *IEEE Transactions on Biomedical Circuits and Systems*, vol. 16, no. 5, pp. 882-890, Oct. 2022.

[69] J. Xiong, H. Zhang, H. Hong, H. Zhao, X. Zhu, and C. Li, "Multi-target vital signs detection using SIMO continuous-wave radar with DBF technique," *Proc. IEEE Radio Wireless Symp. (RWS).*, pp. 194-196, Jan. 2020.

[70] S. Shi, Y. Xie, M. Li, A. X. Liu, and J. Zhao, "Synthesizing Wider Wi-Fi Bandwidth for Respiration Rate Monitoring in Dynamic Environments," *in Proc. IEEE INFOCOM.*, 2019, Paris, France, pp. 874?882, Apr. 2019.

[71] A. Zhu, X. Qi, T. Fan, Z. Gu, Q. Lv, D. Ye, J. Huangfu, Y. Sun, W. Zhu, and L. Ran, "Indoor localization for passive moving objects based on a redundant SIMO radar sensor," *IEEE J. Emerg. Sel. Topics Circuits Syst.*, vol. 8, no. 2, pp. 271?279, Jun. 2018.

[72] Y. Zhang, Y. Ma, X. Yu, P. Wang, H. Lv, F. Liang, Z. Li and J. Wang, "A coarse-to-fine detection and localization method for multiple human subjects under through-wall condition using a new telescopic SIMO UWB radar," *Sensors and Actuators A Physical.*, 332, 2021, 113064.

[73] N.Shiraki, N.Honma, K.Murata, T.Nakayama, and S.Iizuki, "Estimation method of the number of targets using cooperative multi-static MIMO radar," *IEICE Trans. Commun*, vol.E104-B, no.12, Dec. 2021.

Acknowledgement

I would like to thank Professor Naoki Honma and Assistant Professor Kentaro Murata for their courteous guidance in compiling this paper. They are consistently allowed this paper to be my own work, but steered me in the right the direction whenever they thought I needed it. I would also like to express my sincere gratitude to Professor Masahiro Daibo and Professor Koichiro Kobayashi for their advice and cooperation.

I would also like to thank Takeshi Nakayama and Shoichi Iizuka of the Panasonic Corporation for the technical support, and Nobuyuki Shiraki of the Honma and Murata Laboratory for a lot of precious advices and cooperation in this research. Without their passionate participation and input, the validation survey wouldn't have successfully conducted.

Finally, I must express my very profound gratitude to my parents and to each member of the Honma and Murata Laboratory for providing me with unfailing support and continuous encouragement throughout my years of study and through the process of researching and writing this thesis. This accomplishment would not have possible without them. Thank you.

Publications
1. Journal paper

[1] A. Abuduaini, N. Shiraki, N. Honma, T. Nakayama and S. Iizuka, "Frequency Error Compensation of Unsynchronized Bistatic CW- MIMO Radar for Multiple Human-Body Localization," IEEE Transactions on Biomedical Circuits and Systems, vol. 16, no. 5, pp. 882-890, Oct. 2022, doi: 10.1109/TBCAS.2022.3205362.

[2] A.Abudusaimi, N. Shiraki, N. Honma, D. Sasakawa, T. Nakayama, S. Iizuka, "SIMO Antenna Array Based Indoor Localization Technique of Multiple Human-Bodies Using Roundtrip Channels," IEEE OJAP. submitted.

Publications
2. International conference

[1] Abudusaimi abuduaini, et.al,"Performance evaluation of multiple human-Body localization using bistatic MIMO radar,"2019 APMC Conference, IF-44, September. 2019.

3. Domestic conference

[1] Abudusaimi abuduaini, et.al, " Human-Body Localization Using Unsynchronized MIMO Radar, " IEICE General Conference, B-1-41, March. 2019.

[2] Abudusaimi abuduaini, et.al, " Performance Analysis of Unsynchronized MIMO Radar for Human-Body Localization, " IEICE Joint Convention of Tohoku Section, 1I05, August. 2019.

[3] Abudusaimi abuduaini, et.al, " Localization Performance of Unsynchronized MIMO Radar with Multiple Human-bodies, " IEICE Society Conference, B-1-85, September. 2019.

[4] Abudusaimi abuduaini, et.al, "Localizing Multiple Human-Bodies Using Unsynchronized Bistatic MIMO Radar, " IEICE, AP2019-76, pp.37-42, September. 2019.

[5] Abudusaimi abuduaini, et.al, "Experimental evaluation of human-body localization using bidirectional SIMO channel," IEICE Society Conference, B-1-90, September. 2022.

[6] Abudusaimi abuduaini, et.al, " Frequency adjustment for human-body localization using bidirectional SIMO channel ," IEICE MW, AP33, October. 2022.

[7] Abudusaimi abuduaini, et.al, "Experimental analysis of multiple targets' detection performance of bidirectional SIMO radar " IEICE General Conference, B-1-132, March. 2023.

4. Award

[1] IEEE Sendai Section The Best Paper Prize, Dec. 2019.